Article

Structure-based design and biological characterization of selective histone deacetylase 8 (HDAC8) inhibitors with anti-neuroblastoma activity

Tino Heimburg, Fiona R. Kolbinger, Patrik Zeyen, Ehab Ghazy, Daniel Herp, Karin Schmidtkunz, Jelena Melesina, Tajith Baba Shaik, Frank Erdmann, Matthias Schmidt, Christophe Romier, Dina Robaa, Olaf Witt, Ina Oehme, Manfred Jung, and Wolfgang Sippl

J. Med. Chem., **Just Accepted Manuscript** • DOI: 10.1021/acs.jmedchem.7b01447 • Publication Date (Web): 30 Nov 2017

Structure-based design and biological characterization of selective histone deacetylase 8 (HDAC8) inhibitors with anti-neuroblastoma activity

Tino Heimburg[1], *Fiona R. Kolbinger*[2,3], *Patrik Zeyen*[1], *Ehab Ghazy*[1], *Daniel Herp*[4], *Karin Schmidtkunz*[4], *Jelena Melesina*[1], *Tajith Baba Shaik*[5], *Frank Erdmann*[1], *Matthias Schmidt*[1], *Christophe Romier*[5], *Dina Robaa*[1], *Olaf Witt*[2,3,6], *Ina Oehme*[2,3], *Manfred Jung*[4], *and Wolfgang Sippl*[1]*

[1]Institute of Pharmacy, Martin-Luther University of Halle-Wittenberg, 06120 Halle/Saale, Germany

[2]Clinical Cooperation Unit Pediatric Oncology, German Cancer Research Center (DKFZ), INF 280, D-69120 Heidelberg, Germany and German Consortium for Translational Cancer Research (DKTK)

[3]Translational Program, Hopp Children's Cancer Center at NCT Heidelberg (KiTZ)

[4]Institute of Pharmaceutical Sciences, University of Freiburg, 79104 Freiburg, Germany

[5]Département de Biologie Structurale Intégrative, Institut de Génétique et Biologie Moléculaire et Cellulaire (IGBMC), Université de Strasbourg (UDS), CNRS, INSERM, 67404 Illkirch Cedex, France

[6]Department of Pediatric Oncology, Hematology and Immunology, University of Heidelberg Medical Center

Keywords : HDAC8, structure-based design, neuroblastoma, benzhydroxamic acids

ABSTRACT

Histone deacetylases (HDACs) are important modulators of epigenetic gene regulation and additionally control the activity of non-histone protein substrates. While for HDACs 1-3 and 6 many potent selective inhibitors have been obtained, for other subtypes much less is known on selective inhibitors and the consequences of their inhibition. The present report describes the development of substituted benzhydroxamic acids as potent and selective HDAC8 inhibitors. Docking studies using available crystal structures have been used for structure-based optimization of this series of compounds. Within this study, we have investigated the role of HDAC8 in the proliferation of cancer cells and optimized hits for potency and selectivity, both in vitro and in cell culture. The combination of structure-based design, synthesis, in vitro screening to cellular testing resulted in potent and selective HDAC8 inhibitors that showed anti-neuroblastoma activity in cellular testing.

INTRODUCTION

Neuroblastoma, the most common extracranial solid tumor occurring in childhood, arises from abnormal growth of the neuronal crest progenitor cells of the devolving sympathetic nervous system. A distinguishing mark of neuroblastoma is its highly heterogeneous clinical behavior, which ranges from spontaneous tumor regression to highly aggressive, treatment-resistant and fatal tumor progression. Despite numerous advances and the implementation of intensive multimodal therapies, the prognosis for patients with high risk disease, which represent almost half of all neuroblastoma patients, still remains poor with less than 50% long-term survival rates.[1] Further, high risk patients suffer from severe treatment-related immediate and long-term adverse effects, and a significant number will still relapse.[2-3] This emphasizes the urgent need for novel, more effective, and less toxic therapeutic approaches to improve the survival and the life-quality of neuroblastoma patients. Diverse genomic abnormalities have been described in neuroblastoma,

yet no common genomic aberration has been uniformly identified in all high risk patients. One of the most important genetic marks of neuroblastoma is the amplification of the proto-oncogene MYCN [4-6] which is usually associated with tumor aggressiveness, resistance to therapy, and poor survival.[3, 7] Besides MYCN, *ALK* has also been implicated as another causative gene in neuroblastoma; activation mutations of ALK occur in all cases of familial neuroblastoma and in ca. 14% of sporadic cases.[8-9] Other recurrent genetic alterations include deletions on chromosomes 1p and 11q or gains on 17q, which are all used as prognostic markers.[10]

HDAC inhibitors are an emerging class of drugs which have shown promise in the treatment of a wide variety of malignancies.[11-13] We have previously demonstrated that specifically the isozyme HDAC8 is involved in the pathogenesis of neuroblastoma and that its expression significantly correlates with advanced tumor stage and markers for poor prognosis.[14]

HDAC8 is a 42 kDa protein composed of 377 amino acids, which is ubiquitously expressed and located in the nucleus and in the cytoplasm, where it supports smooth muscle cell differentiation and contractility by interaction with α-actin and modulators of cytoskeleton dynamics.[15-16] Histones are not considered to be bona fide HDAC8 substrates and acetylation patterns observed in vitro and in cells regularly differ.[17] While SMC3, a cohesin complex protein exerting its role during the separation of sister chromatids, is directly deacetylated by HDAC8, the enzyme can also interact with other proteins as a scaffold.

HDAC8 plays a significant role in regulating spindle assembly during mouse oocyte meiosis.[18] In oral squamous cell carcinoma cells, HDAC8 knockdown induced apoptotic cell death through caspases activation and pro-survival autophagy, consequently, the additional treatment with autophagy inhibitors enhanced cell death.[19]

HDAC8 has also been shown to be one of the causative genes in Cornelia de Lange syndrome (CdLS), a rare genetic disease causing congenital malformations, and has been identified as

SMC3 deacetylase.[20] Chromatin-released acetylated SMC3 is deacetylated by the HDAC8 enzyme in early mitosis facilitating cohesin recycling for subsequent cell cycles. There have been several loss-of-function mutations reported for HDAC8, that result in a strong loss of activity.[21] Therefore, specific HDAC8 activators, such as *N*-(phenylcarbamothioyl)benzamide, have been reported as useful leads in the search for new therapeutic strategies in managing CdLS.[22]

In INSS stage 4 neuroblastoma patient samples, HDAC8 is the only HDAC isoform showing significant transcriptional upregulation as compared to stages 1, 2, 3 and 4S. High HDAC8 levels were found to be correlated with predictors of poor prognosis in neuroblastoma such as unfavorable Shimada histopathologic classification and loss of chromosomes 1p and 11q.[14] Zhao et al. revealed that targeted inhibition of HDAC8 by subtype-selective HDAC8 inhibitors such as PCI-34051[23] (**1**, Figure 1) can suppress the growth of neuroblastoma cells and increase Doxorubicin sensitivity via upregulation of miR-137 and suppression of MDR1.[24] The pivotal role of this class I HDAC in differentiation and tumor progression has been confirmed in malignant peripheral nerve sheath tumors[25] and neuroblastoma, where selective HDAC8 inhibition induces a differentiated phenotype, enhances retinoic acid-mediated effects, and reduces tumor growth in cell culture and in vivo with decreased adverse effects as compared to unspecific HDAC inhibition.[26] This endorses selective HDAC8 inhibition as a very promising therapeutic option for neuroblastoma therapy.

The FDA-approved broad-spectrum HDAC inhibitor vorinostat (SAHA), which is used to treat refractory cutaneous T-cell lymphoma, is a weaker inhibitor of HDAC8 (micromolar range) than of HDACs 1–3 (nanomolar range). Selective HDAC8 inhibitors were identified by either structure-based design, for example, linkerless hydroxamic acids (IC_{50} 0.3 μM, >100-fold selectivity over HDAC1 and 6)[27] or from high-throughput screens like the cyclic thiourea SB379278A (IC_{50} 0.5 μM)[28] (Figure 1).[29] Compound **1** (Figure 1) is probably the most widely

used HDAC8-specific inhibitor in research. Based on an indole linker, this hydroxamic acid showed good HDAC8 selectivity and cellular activity.[23] NCC149 (Figure 1) and further analogs were identified using a rapid screen of a 151-triazole compound library generated using click chemistry.[30-31] In vitro tests revealed an IC_{50} of 70 nM against HDAC8 with a very high selectivity over major HDACs (HDAC1: IC_{50} 38 μM, HDAC2 >100 μM, HDAC4: IC_{50}: 44 μM, HDAC6: IC_{50} 2.4 μM). Huang et al. reported *ortho*-aryl-*N*-hydroxycinnamides as further selective HDAC8 inhibitors.[32] The biphenyl substituted *ortho*-aryl-*N*-hydroxycinnamide (Figure 1) showed an IC_{50} value of 27 nM for HDAC8, good selectivity over other HDACs and moderate growth inhibition of lung cancer cell lines. Tang et al. reported on the synthesis of a small library of benzhydroxamic acids containing a hydrazide linker.[33] The most promising compound A8B4 (Figure 1) showed an IC_{50} of 23 nM and good selectivity over HDAC2 and HDAC3. However, no cellular data was reported. Very recently, Ingham et al. developed a highly potent HDAC8 inhibitor with good selectivity over HDAC1 and HDAC6. The triazole hydroxamic acid OJI-1 (Figure 1) showed an IC_{50} of 0.8 nM.[34] However, no cellular data has been provided so far.

Besides hydroxamic acids, inhibitors containing an amino acid group[35] and an azetidinone group[36] were reported as selective HDAC8 inhibitors (Figure 1). Another potent, non-hydroxamic acid HDAC8 inhibitor, that has been reported, is β-phenyltropolone.[37] The beta-isopropyltropolone derivative showed a *K*i of 8 nM and about 1400-fold selectivity toward HDAC8 than HDAC4. Synthetic as well as structure-based approaches to develop benzhydroxamic acids as HDAC8 inhibitors have been recently reported and reviewed.[38-39]

Based on our previous study[40] to develop inhibitors of *Schistosoma mansoni* HDAC8, we identified the benzhydroxamic acids **2**, **3**, and **4** (Figure 2; IC_{50} values are listed in Table 1) as promising starting points for the development of inhibitors of the homologous human HDAC8. Our previous results showed that the lead benzamido-hydroxamic acid **2** displays good inhibition

of hHDAC8, high selectivity over HDAC1 and a moderate selectivity over HDAC6. Modifying the capping group to quinoline and introducing a methyl substituent in the *para*-position of the benzhydroxamic acid moiety (**3**) resulted in a significant improvement in HDAC8 inhibition but was coupled with a loss of selectivity towards HDAC6. Meanwhile, switching from an amide- to an amine-linker (**4**) resulted in a considerable enhancement of HDAC8 inhibition, but simultaneously a decreased selectivity against HDAC1 was observed as compared to **2**.

On the basis of our initial data, we wanted to get insights into the structure-activity relationships (SARs) of HDAC8 inhibitors with a *meta*-substituted benzhydroxamic acid structure. Here we report that changes of the linker attached to the benzhydroxamic acid have a huge impact on HDAC8 potency and selectivity (Figure 3). In addition, anti-neuroblastoma activity of the most promising inhibitors was verified by viability and colony formation assays as well as detection of neurite-like outgrowths and upregulation of differentiation markers, such as p21/CDKN1, TrkA/NTRK1 and tyrosine hydroxylase (TH).

CHEMISTRY

In order to obtain the described 3-aminobenzhydroxamic acids (**8a-s**), both non-substituted and 4-substituted-3-aminobenzoic acids (**5a-s**) were used as starting points. Alkyl and aryl residues were introduced on the aromatic NH_2 group via reductive amination, which was performed by the reaction of the 3-aminobenzoic acids **5a-s** with the respective aldehyde using sodium triacetoxyborohydride as a reducing agent.[40] To avoid byproducts in the following synthetic steps, the secondary amine **6** was protected by *tert*-butyloxycarbonyl (Boc) group initially (Scheme 1). However, we recognized in further trials that this step could be skipped because the byproducts were only obtained in small amounts and could be neglected. The *N*-phenethyl substituted derivatives **6l** and **6s** were alternatively attained through *N*-alkylation since the products of the reductive amination using phenylacetaldehyde and sodium triacetoxyborohydride

showed poor purity. The desired hydroxamic acids **8a-s** were finally obtained using PyBOP as an activating agent and *O*-(tetrahydro-2*H*-pyran-2-yl)hydroxylamine followed by cleavage of the protecting group (Scheme 1). Generally, using tetrahydropyran (THP)-protected hydroxylamine increased the yields of the desired benzhydroxamic acids compared to other methods using hydroxylamine hydrochloride and KOH or potassium methanolate.

The desired phenylcarbamoyl-benzhydroxamic acids **12a-d** could be obtained starting from the methoxycarbonylbenzoic acid derivatives **9a-d**, which were first activated using thionyl chloride or oxalyl chloride and subsequently coupled with the respective aniline to yield the corresponding amides **10a-d**. Alkaline hydrolysis of the methyl ester to the respective 3-substituted carbamoylbenzoic acid **11a-d** was followed by the conversion to the hydroxamic acids **12a-d** using the aforementioned protocol. While the 3-phenyl-4-carbamoylbenzoic acid **11a** could be directly prepared from the commercially available 3-methoxycarbonylbenzoic acid **9a** using thionyl chloride and coupling with aniline, the starting materials 5-methoxycarbonyl-2-substituted-benzoic acids **9b-d** had to first be prepared as described in literature (see Scheme S1 Supporting Information). [41] Activation of the three acids **9b-d** was achieved using oxalyl chloride as a mild and efficient activating agent. The activated acid chlorides were then coupled with 4-chloroaniline using DIPEA as a base to form the respective amides **10b-d** (Scheme 2).

The 3-benzyloxy-4-methoxybenzhydroxamic acid **20a** was directly synthesized from the commercially available carboxylic acid **25** using the aforementioned procedure (Scheme 3). To obtain **20b-g**, the acid derivatives **21** were first converted to the methyl esters **22** to avoid byproducts in the following steps. *O*-Benzylation to the ether derivatives **24b-g** was performed through Williamson-ether-synthesis using K_2CO_3 and the respective substituted benzyl bromides **23**.[42] The corresponding 3-benzyloxy-benzhydroxamic acids **20b-g** were synthesized by cleavage

of the methyl ester followed by the conversion of the carboxylic acid as previously described (Scheme 3).

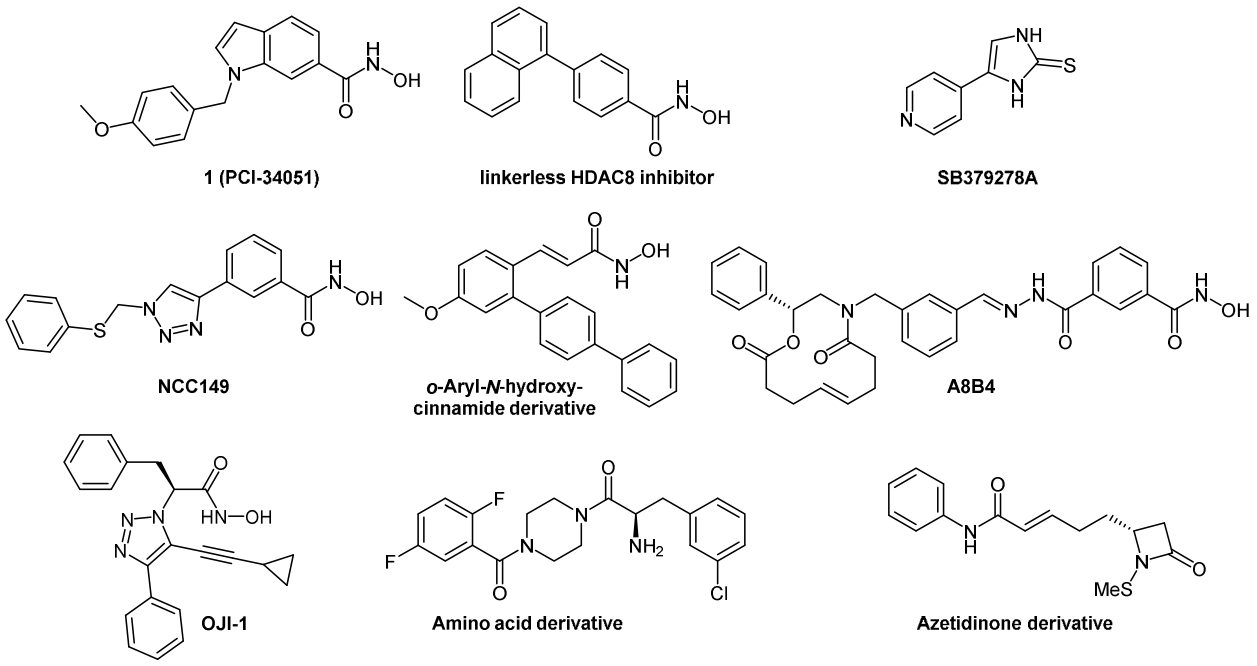

Figure 1. Chemical structures of HDAC8 inhibitors.

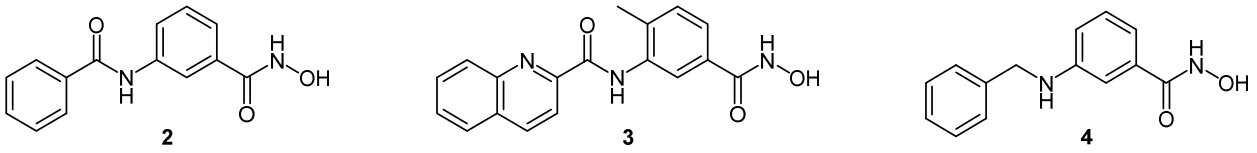

Figure 2. Previously identified benzhydroxamic acid-based HDAC8 inhibitors**.**

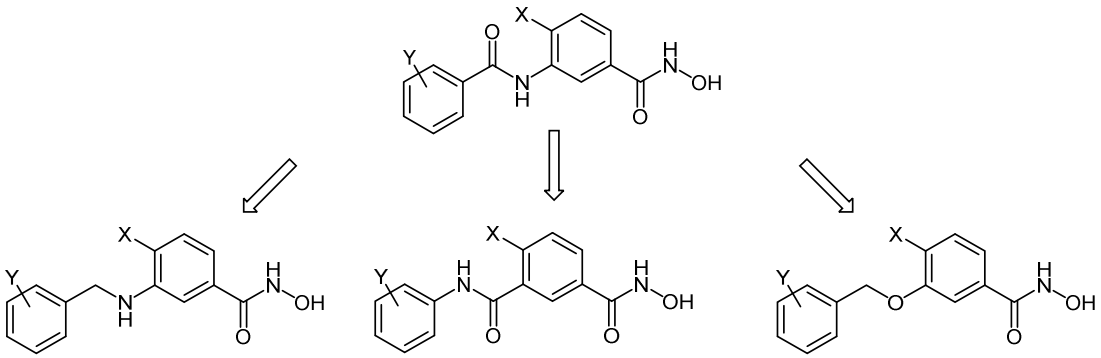

Figure 3. Series of the herein described benzhydroxamic acids as HDAC8 inhibitors.

Scheme 1.

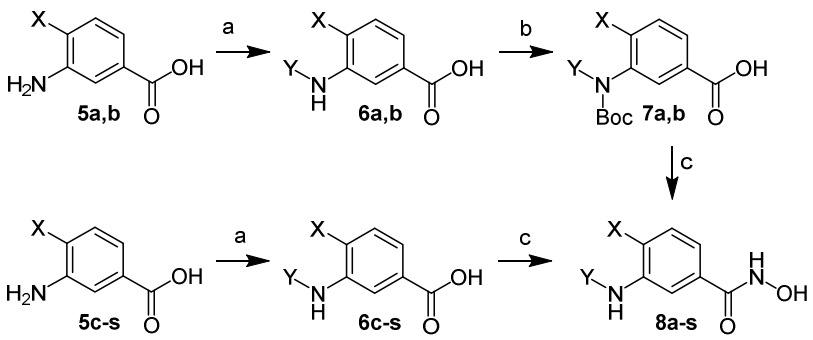

8a: X = methyl; Y = benzyl
8b: X = methoxy; Y = benzyl
8c: X = methyl; Y = 2-chlorobenzyl
8d: X = methyl; Y = 4-chlorobenzyl
8e: X = methyl; Y = 2,6-dichlorobenzyl
8f: X = methyl; Y = 2,4-dichlorobenzyl
8g: X = methoxy; Y = 3-methoxybenzyl
8h: X = methoxy; Y = 3-phenoxybenzyl
8i: X = methoxy; Y = 2-quinolinylmethyl
8j: X = methoxy; Y = 4-chlorobenzyl
8k: X = methoxy; Y = 1-(4-chlorophenyl)ethyl
8l X = methyl; Y = 2-phenylethyl
8m: X = chloro; Y = benzyl
8n: X = ethyl; Y = benzyl
8o: X = fluoro; Y = benzyl
8p: X = methyl; Y = 4-phenylbenzyl
8q: X = methyl; Y = 2-naphtylmethyl
8r: X = methoxy; Y = 2-phenylethyl
8s: X = methyl; Y = 3-phenylpropyl

(a) i. aldehyde, toluene; ii. $Na(AcO)_3BH$, AcOH; (b) Boc_2O, MeOH, *t*-BuOH; (c) i. PyBOP, DIPEA, H_2NOTHP, THF; ii. cat. HCl, THF; (7a,b) iii. TFA, $CHCl_3$

Scheme 2.

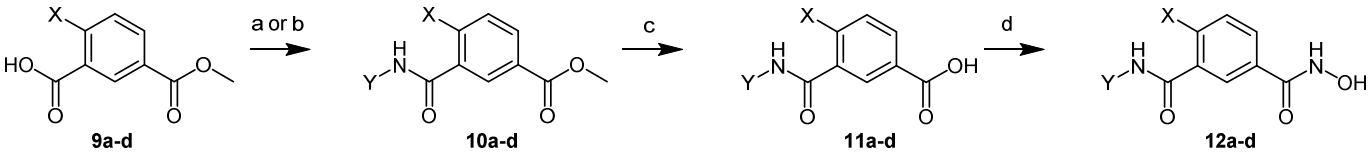

12a: X = H; Y = phenyl
12b: X = methoxy; Y = 4-chlorophenyl
12c: X = chloro; Y = 4-chlorophenyl
12d X = methyl; Y = 4-chlorophenyl

(a) $SOCl_2$, aniline; (b) $(COCl)_2$, 4-chloroaniline, cat. DMF, DIPEA, CH_2Cl_2 (c) aq. NaOH, MeOH; (d) i. PyBOP, DIPEA, H_2NOTHP, THF; ii. cat. HCl, THF

Scheme 3.

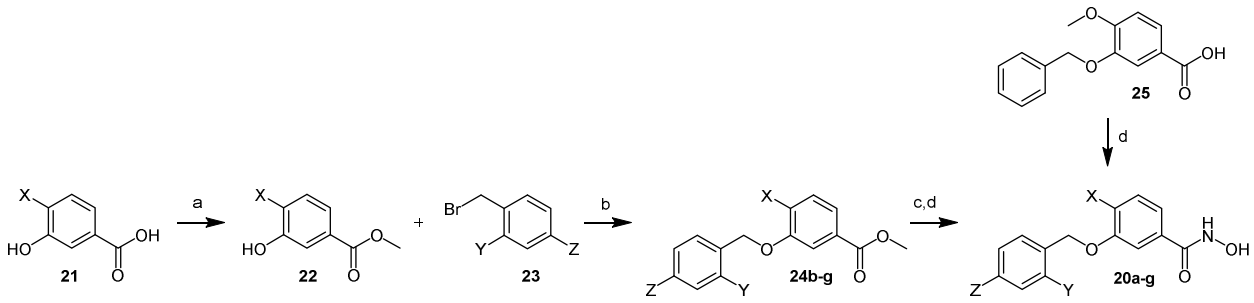

20a: X = methoxy; Y = H; Z = H
20b: X = methoxy; Y = H; Z = chloro
20c: X = methoxy; Y = chloro; Z = H
20d: X = methoxy; Y = chloro; Z = chloro
20e: X = chloro; Y = H; Z = chloro
20f: X = chloro; Y = choro; Z = H
20g: X = chloro; Y = chloro; Z = chloro

(a) $SOCl_2$, MeOH; (b) K_2CO_3, DMF; (c) aq. NaOH, MeOH; (d) PyBOP, DIPEA, H_2NOTHP, THF; cat. HCl, THF

STRUCTURE-ACTIVITY RELATIONSHIPS

Initial optimization studies focused on the linker between the benzhydroxamic acid and the terminal aromatic ring used as capping group. Our previously reported lead benzamido-hydroxamic acid **2**[40] showed a moderate HDAC8 inhibitory activity as compared to the selective HDAC8 inhibitor **1** (Table 1) and exhibited a good selectivity profile against HDAC1 and to a lesser extent HDAC6. As previously described, switching from an amide- to an amine-linker (compound **4,** Table 1) resulted in a slight improvement in the HDAC8 inhibitory potency, a considerable loss in the selectivity over HDAC1 and a slight increase in the selectivity over HDAC6.

In order to guide further optimization efforts, docking studies were performed using the lead structures in available crystal structures of HDAC8 (PDB ID: 2V5X[43]), HDAC1 (PDB ID: 4BKX[44]) and HDAC6 (PDB ID: 5EDU[45] and 5G0I[46]), in an attempt to detect the structural aspects determinant for achieving high HDAC8 inhibitory potency as well as selectivity over HDAC1 and -6. As could be expected, the benzhydroxamic acid group of all lead compounds showed a similar interaction pattern in the catalytic pocket of HDAC8: The hydroxamic acid group is able to chelate the zinc ion in a bidentate fashion and undergo three H-bond interactions

with the side chains of His142, His143 and Tyr306. Meanwhile the benzene ring is sandwiched between Phe152 and His180, where it exhibits π-π stacking interactions. The capping group of the different leads showed, however, more diverse interactions, which might give a primary explanation for the differences in the HDAC8 inhibitory activity. The benzyl moiety of **1** exhibits π-π stacking interactions with Tyr306 and Phe152, which are lost in the case of the less potent benzamide derivative **2**. The corresponding highly active quinoline derivative **3** seems to benefit from additional hydrophobic interactions with Tyr306 and Pro273, while the 3-aminobenzhydroxamic acid **4** shows, like **1**, π-π stacking interactions with Tyr306 and Phe152. (Figure 4)

The selectivity of the compounds over HDAC1 could be easily explained by the docking results (see Supporting Information Figure S1) which clearly show that the compounds are not able to properly chelate the catalytic zinc ion. HDAC1 is characterized by its narrow pocket as compared to HDAC8 and -6, and, hence, *meta*-substituted benzhydroxamic acids generally show a HDAC6/8 over HDAC1 selectivity as has been frequently demonstrated in previous studies.[31, 40, 47-49]

Meanwhile, the docking results cannot completely rationalize the selectivity of the compounds for HDAC8 over HDAC6. Crystal structures of HDAC6 and HDAC8 clearly demonstrate that the substrate binding grooves in both isoforms show a significantly different shape, with one of the main differences in HDAC6 being the presence of an additional loop (L1-loop: Asp460-Pro464, DrHDAC6 numbering). While in HDAC8 the benzyl capping group of **1** is placed perpendicular to Tyr306 and Phe152 allowing for a perfect π-π stacking interaction, the additional loop in HDAC6 hinders the ligand from binding to this hydrophobic subpocket. In the case of **1**, only a hydrophobic interaction with Leu712 of HDAC6 can be observed. The benzamido-hydroxamic acids **2** and **3** seem to benefit from additional water-mediated H-bond interactions with the

conserved water molecule at the rim of the catalytic tunnel. Interestingly, the quinoline group of **3** is able to undergo additional hydrophobic interactions which extend to Pro464 of the L1-loop, which might explain the observed increase in HDAC6 inhibitory potency. Meanwhile, due to the flexibility of the aminomethyl linker of compound **4**, the capping benzyl group can undergo π-π stacking interactions with Phe583 (see Supporting Information Figure S2).

In order to obtain more potent and selective HDAC8 inhibitors, we started with the derivatization of the 3-amino-benzhydroxamic acid **4** by introducing different substituents at the 4-position of the benzhydroxamic acid core and modifying the capping groups to maximize the interactions in the previously described hydrophobic side pocket of HDAC8.

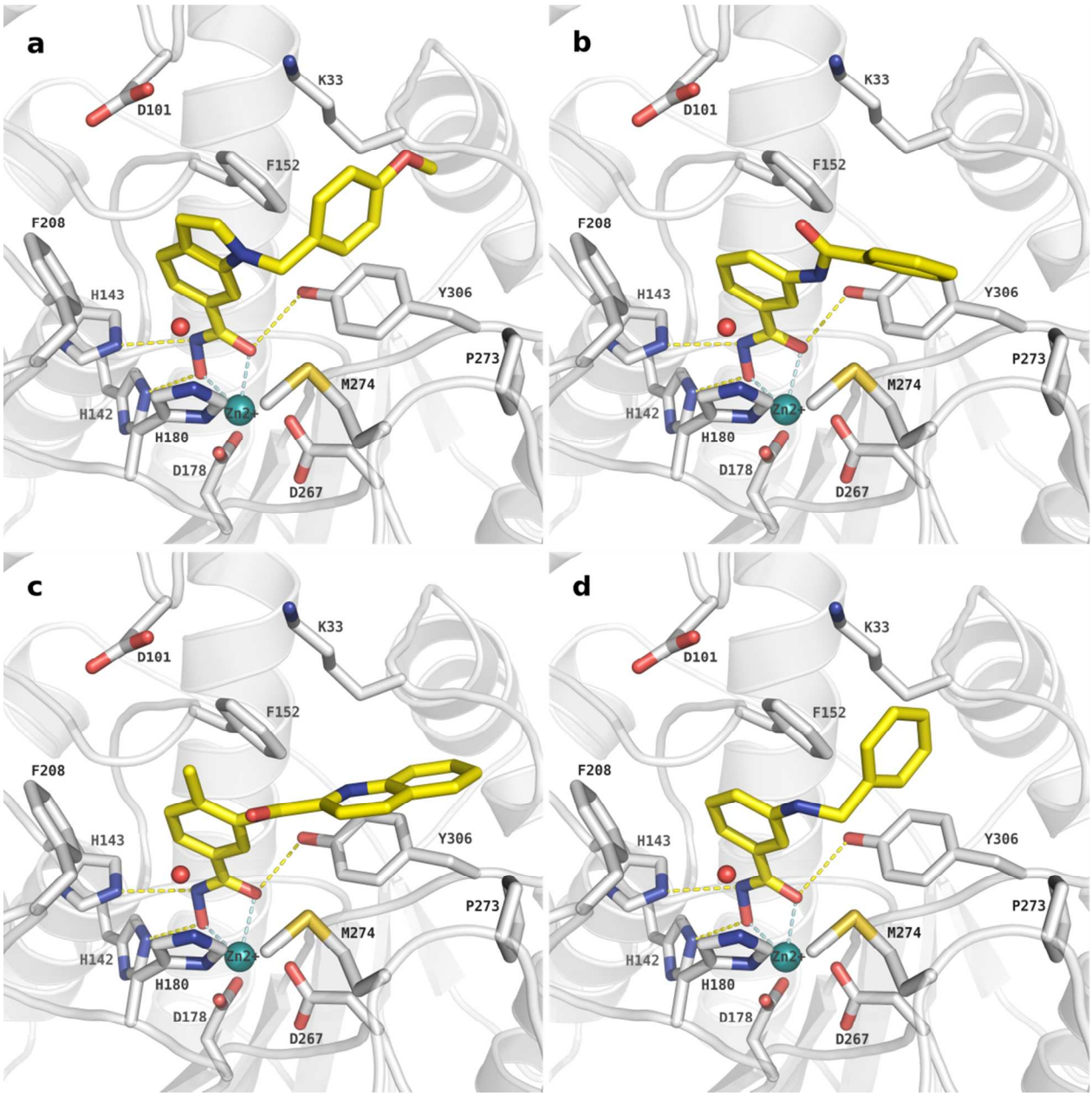

Figure 4. Predicted binding modes in HDAC8: a) the reference inhibitor **1**, b) the benzamido-hydroxamic acid **2**, c) the corresponding quinoline derivative **3**, and d) the 3-aminobenzhydroxamic acid derivative **4**. Side chains of active site residues are shown as white sticks and the ligands as yellow sticks. The zinc ion is depicted as cyan ball, while cocrystallized water molecules are shown as red spheres. Hydrogen bonds are shown as yellow dashed lines and coordination of the zinc ion as pale-cyan dashed lines.

Regarding the 3-amino-benzhydroxamic acid series (**8a-s**), the introduction of a hydrophobic substituent in the *para*-position of the benzhydroxamic acid moiety generally resulted in a decreased inhibitory activity against HDAC1 as compared to the unsubstituted derivative **4**, however, had little impact on the HDAC6 activities (Table 2). Only compounds with a methoxy (**8b**) and a fluoro substituent (**8o)** showed increased HDAC8 inhibitory activity and consequently higher selectivity over HDAC1 and -6, as compared to the respective 4-methyl and the unsubstituted derivative (**8a** and **4**). Docking of **8b** to HDAC8 shows that it adopts a highly similar binding conformation as that predicted for the unsubstituted 3-aminobenzhydroxamic acid **4**, where the hydroxamic acid group chelates the zinc ion and forms three H-bond interactions with the conserved His and Tyr residues, the core benzene moiety is sandwiched between Phe152 and His180 and the capping benzyl group exhibits π-π stacking interactions with Tyr306 and Phe152. Additionally, the 4-methoxy group can undergo hydrophobic interactions with Phe208 (Figure 5a). Meanwhile, the 4-fluoro derivative **8o** and the 4-chloro derivative **8m** also showed a similar binding mode to **4** (not shown). Whereas the fluoro substitution (**8o)** resulted in a similar inhibitory activity, the chloro substitution (**8m**) was found to be less favourable. However, the obtained docking results offer no explanation for the differences in HDAC8 inhibition. Similarly, increasing the length of the linker to ethylene and propylene moieties (**8k**, **8l**, **8r** and **8s**) did not result in an increase in the inhibitory activity against HDAC8 or an enhancement of the compounds' selectivity. With respect to the capping groups, most of the probed moieties were well tolerated by HDAC8, even bulkier groups like biphenyl (**8p**) and naphthyl (**8q**). A significant enhancement in the inhibitory activity against HDAC8, together with an improvement in the selectivity over HDAC1 and HDAC6, was only observed for the 2,4-dichloro derivative **8f**. This might be explained by the dichlorophenyl capping group undergoing additional vdW interaction with the hydrophobic side pocket of HDAC8 (Figure 5b). Among this series, the 4-

methoxy-benzyl derivative **8b** and the 4-methyl-2,4-dichloro derivative **8f** displayed the highest potency against HDAC8 (IC_{50} 69 nM and 35 nM; respectively) and simultaneously showed the best selectivity over HDAC1 (210 and 534 fold HDAC8/HDAC1; respectively) and HDAC6 (74 and 411 HDAC8/HDAC6; respectively).

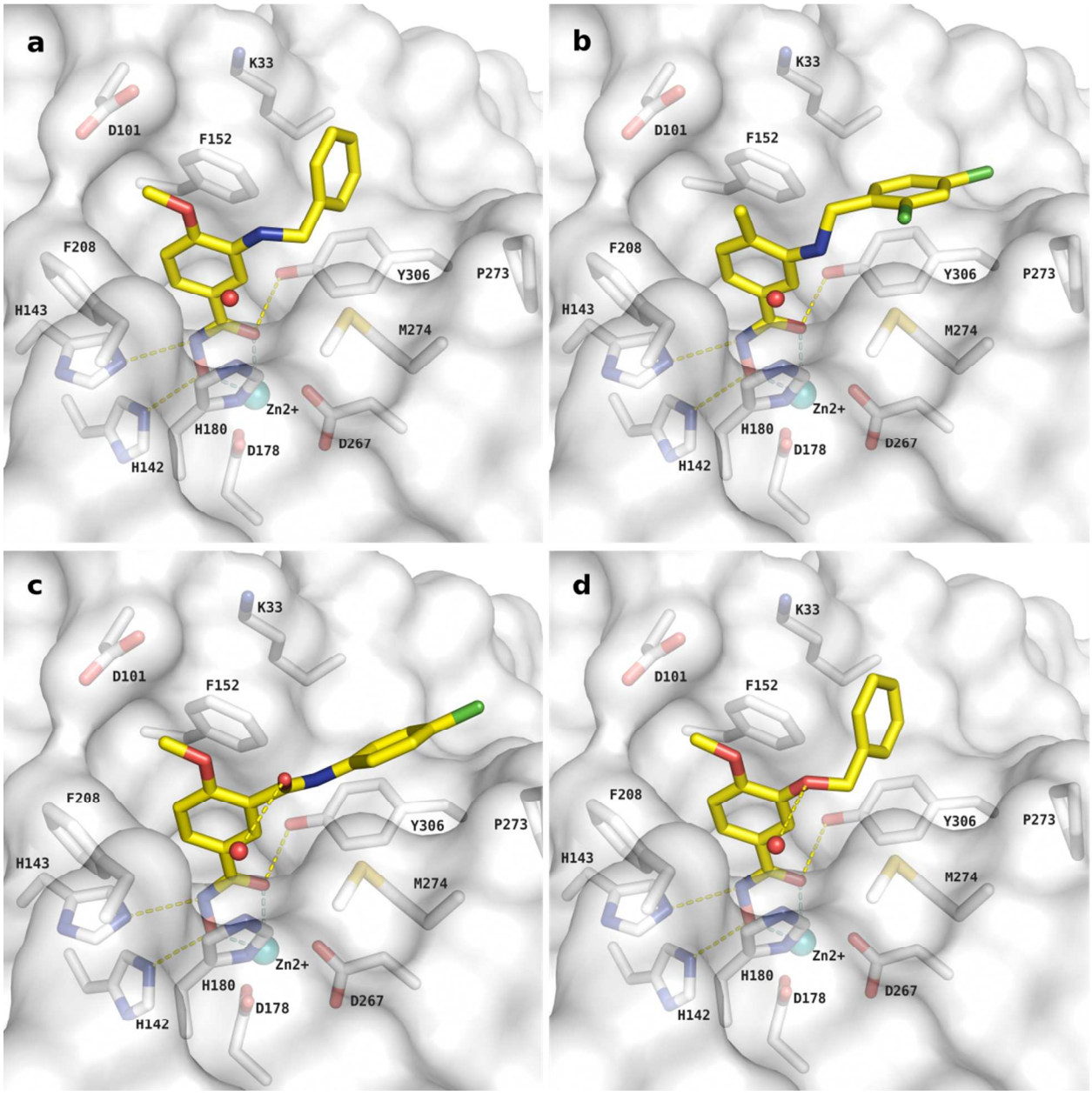

Figure 5. Predicted binding mode of the most potent HDAC8 inhibitors: a) the 4-methoxy-3-benzylamino-benzhydroxamic acid **8b**, b) the 2,4-dichlorobenzylamino-benzhydroxamic acid derivative **8f**, c) the inverted amide derivative **12b**, and d) the 3-benzyloxy-benzhydroxamic acid

derivative **20a** in human HDAC8. Ligands are colored in yellow, side chains of active site residues are shown as white sticks, the zinc ion is depicted as cyan ball, while the cocrystallized water molecule is shown as red balls. Hydrogen bonds are shown as yellow dashed lines and coordination of the zinc ion as pale-cyan dashed lines.

Another series of inhibitors that we prepared was obtained by inverting the amide linker of **2**. The inverted amide **12a** (which has already been reported)[49] showed about four times increased HDAC8 inhibitory activity compared to **2** (Table 3). Adding a methoxy group at the *para*-position of the benzhydroxamic acid and modifying the terminal phenyl ring with a *para*-chloro substituent resulted in a highly potent HDAC8 inhibitor (**12b**, IC_{50} 38 nM), but was coupled with an increase in the inhibition of HDAC1 and -6. Docking studies revealed that the inverted amide is able to benefit from an additional water-mediated H-bond interaction which is missing in the analogous benzamido-hydroxamic acid **2** (Figure 5c). Further modifications did not result in an improvement in the potency against HDAC8. Due to the strong HDAC6 inhibition, we did not further study the most active compound in this series (**12b**; HDAC6: 59% inhibition at 1μM), in the cellular testing.

The third linker that we tested was a methyleneoxy group (Table 4). As described for the 3-aminobenzhydroxamic acids, the *para*-position of the benzhydroxamic acid scaffold was modified and hydrophobic substituents at the terminal benzyl group were used in an attempt to increase the potency of the compounds. The 4-methoxy substituted inhibitor **20a** showed the strongest HDAC8 inhibition among all tested compounds with good selectivity indices (448 fold against HDAC1, 107 fold against HDAC6). Our docking studies revealed that the ether linker in **20a** is able to undergo water-mediated H-bond interaction with the water molecule at the rim of the catalytic tunnel of HDAC8, while the capping benzyl group shows π-π stacking with Phe152 and Tyr306 (Figure 5d). Derivatives bearing a 4-chloro substituent (**20e-g**) showed a decreased

HDAC8 inhibition as compared to their 4-methoxy counterparts. Meanwhile, introducing chloro-substituents at the capping benzyl group generally resulted in a significant loss in the HDAC8 inhibitory activity. Interestingly, a 2,4-dichloro substitution of **20d** and **20g** resulted in a pronounced decrease in HDAC8 inhibitory potency, which is in contrast to our previous observation where a similar substitution of the 3-benzylamino-benzhydroxamic acid scaffold (**8f**) led to an increase in HDAC8 inhibitory activity and improved selectivity.

Among all herein described compounds, the 3-benzylamino-benzhydroxamic acids **8b, 8f,** and the 3-benzyloxy-benzhydroxamic acid **20a** were the most potent and selective compounds in comparison with **1** as reference and were, hence, selected for further biological/cellular testing in comparison with reference inhibitors.

Table 1: In vitro IC_{50} values of reference compounds (values of **2**, **3**, and **4** were taken from Heimburg et al.[40]). (± Standard error, SI = selectivity index).

Cpd. no.	Structure	hHDAC8 IC_{50} nM	hHDAC1 IC_{50} µM	hHDAC6 IC_{50} µM
1	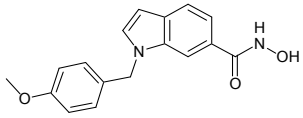	92 ± 15	28.3 ± 2.0 (SI 307)	48.2 ± 6.2 (SI 524)
2	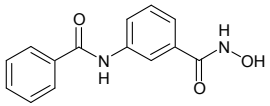	582 ± 48	33.6 ± 1.8 (SI 58)	3.0 ± 0.3 (SI 5)
3	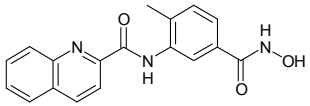	30 ± 7	2.7 ± 0.8 (SI 90)	0.089 ± 0.014 (SI 3)
4	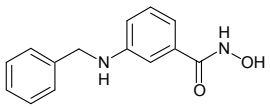	143 ± 7	2.3 ± 1.2 (SI 16)	2.5 ± 1.1 (SI 18)

Table 2. In vitro IC_{50} values of 3-aminobenzhydroxamic acid derivatives. (± Standard error, SI = selectivity index).

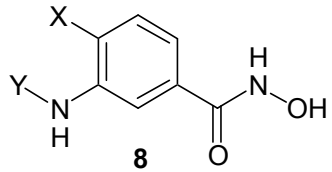

8

Cpd. no.	X	Y	hHDAC8 IC_{50} nM	hHDAC1 % inhibition	hHDAC1 IC_{50} µM	hHDAC6 % inhibition	hHDAC6 IC_{50} µM
8a	methyl	benzyl	260 ± 36	39% @ 25 µM 16% @ 5 µM	21.8 ± 2.1 (SI 84)	69% @ 25 µM 35% @ 5 µM	5.1 ± 0.3 (SI 20)
8b	methoxy	benzyl	69 ± 17	97% @ 100 µM 49% @ 10 µM	14.5 ± 1.4 (SI 210)	70% @ 10 µM 12% @ 1 µM.	5.1 ± 0.8 (SI 74)
8c	methyl	2-chlorobenzyl	286 ± 41	n.d	n.d.	n.d	n.d.
8d	methyl	4-chlorobenzyl	161 ± 21	n.d	n.d.	n.d	n.d.
8e	methyl	2,6-dichlorobenzyl	335 ± 55	32% @ 10 µM 3% @ 1 µM	n.d.	61% @ 10 µM 11 % @ 1 µM	n.d.
8f	methyl	2,4-dichlorobenzyl	35 ± 4	66% @ 50 µM 16% @ 1 µM	18.7 ± 2.5 (SI 534)	75% @ 50 µM 1.6% @ 1 µM	14.4 ± 2.4 (SI 411)
8g	methoxy	3-methoxybenzyl	167 ± 59	31% @ 10 µM	n.d.	38% @ 10 µM	n.d.

				3.5% @ 1 μM		n.i. % @ 1 μM	
8h	methoxy	3-phenoxybenzyl	202 ± 22	32% @ 10 μM 10 % @ 1 μM	n.d.	63% @ 10 μM 11% @ 1 μM	n.d.
8i	methoxy	2-quinolinylmethyl	481 ± 93	45% @ 10 μM 8% @ 1 μM	n.d.	73% @ 10 μM 19% @ 1 μM	n.d.
8j	methoxy	4-chlorobenzyl	147 ± 18	51% @ 10 μM 14 % @ 1 μM	n.d.	59% @ 10 μM 11% @ 1 μM	n.d.
8k	methoxy	1-(4-chlorophenyl)-ethyl	240 ± 22	31% @ 10 μM 5 % @ 1 μM	n.d.	46% @ 10 μM 5% @ 1 μM	n.d.
8l	methyl	2-phenylethyl	130 ± 20	34% @ 10 μM 9% @ 1 μM	n.d.	63% @ 10 μM 20% @ 1 μM	n.d.
8m	chloro	benzyl	254 ± 41	48% @ 10μM 3% @ 1 μM	10.4 ± 1.2 (SI 41)	74% @ 10μM 22% @ 1 μM	4.0 ± 0.2 (SI 16)
8n	ethyl	benzyl	136 ± 17	33% @ 10 μM 8% @ 1 μM	n.d	62% @ 10 μM n.i. @ 10 μM	n.d
8o	fluoro	benzyl	72 ± 12	40% @ 10 μM n.i. @ 1 μM	25.0 ± 6.5 (SI 347)	67% @ 10 μM 20%. @ 1 μM	5.0 ± 0.7 (SI 69)
8p	methyl	4-phenylbenzyl	227 ± 54	43% @ 10 μM 5% @ 1 μM	n.d.	58% @ 10μM 11% @ 1 μM	n.d.

8q	methyl	2-naphtylmethyl	119 ± 34	37% @ 10 μM 8% @ 1 μM	n.d.	52% @ 10 μM 11%. @ 1 μM	n.d.
8r	methoxy	2-phenylethyl	151 ± 33	41% @ 10 μM 0% @ 1 μM	19.1 ± 3.0 (SI 126)	63% @ 10 μM 20% @ 1 μM	7.5 ± 2.8 (SI 50)
8s	methyl	3-phenylpropyl	248 ± 52	29% @ 10 μM 3% @ 1 μM	25.6 ± 5.5 (SI 103)	55% @ 10 μM 42% @ 1 μM	8.9 ± 1.7 (SI 36)

Table 3: In vitro IC_{50} values of 3-(phenylcarbamoyl)benzhydroxamic acid derivatives. (± Standard error, SI = selectivity index)..

Cpd. no.	Structure	hHDAC8 IC_{50} nM	hHDAC1 % inhibition	hHDAC1 IC_{50} µM	hHDAC6 % inhibition	hHDAC6 IC_{50} µM
12a*	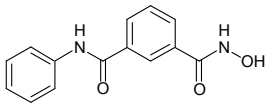	120 ± 37 (110 ± 47)[49]	10% @ 5 µM 3% @ 0.5 µM	39.1 ± 8.9 (SI 326)	80% @ 5 µM 27% @ 0.5 µM	3.1 ± 0.1 (SI 25)
12b	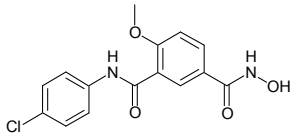	38 ± 2	72% @ 10 µM 24 % @ 1 µM	n.d.	93% @ 10 µM 59 % @ 1 µM	n.d.
12c	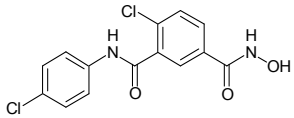	175 ± 45	26% @ 10 µM 0.1 % @ 1 µM	n.d.	78% @ 10 µM 25 % @ 1 µM	n.d.
12d	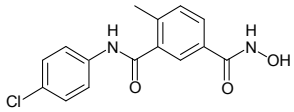	114 ± 14	15% @ 10 µM 1.8 % @ 1 µM	n.d.	69% @ 10 µM 18 % @ 1 µM	n.d.

* IC_{50} value of compound **12a** was previously reported by Olson et. al.[49] Difference in the herein determined IC_{50} value to the reported one might be due to the use of different substrates.

Table 4. In vitro IC_{50} values of 4-benzyloxy-3-substituted-benzhydroxamic acid derivatives. (± Standard error, SI = selectivity index).

Cpd. no.	Structure	hHDAC8 IC_{50} nM	hHDAC1 % inhibition	hHDAC1 IC_{50} µM	hHDAC6 % inhibition	hHDAC6 IC_{50} µM
20a	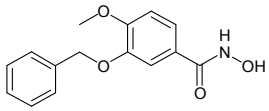	27 ± 3	62% @ 25 µM 34% @ 5 µM	12.1 ± 5.7 (SI 448)	73% @ 25 µM 53% @ 5 µM	2.9 ± 0.3 (SI 107)
20b	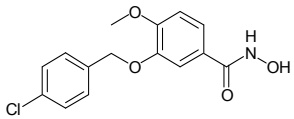	181 ± 26	45% @ 10 µM 8.7% @ 1 µM	14.5 ± 3.5 (SI 80)	78% @ 10 µM 32% @ 1 µM	4.6 ± 0.4 (SI 25)
20c	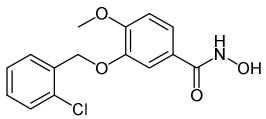	120 ± 20	n.d.	n.d.	n.d.	n.d.
20d	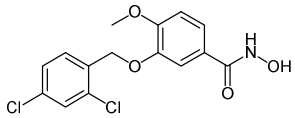	840 ± 120	n.d.	n.d.	n.d.	n.d.
20e	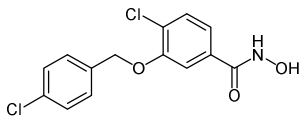	1020 ± 100	n.d.	n.d.	n.d.	n.d.
20f	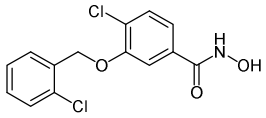	2100 ± 445	n.d.	n.d.	n.d.	n.d.

20g	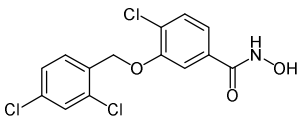	4150 ± 700	n.d.	n.d.	n.d.	n.d.

Table 5. Cytotoxicity studies in HEK293 cells.

Cpd. no.	Viability* (%)	Cpd. no.	Viability* (%)	Cpd. no.	Viability* (%)	Cpd. no.	Viability* (%)
2	72.0 ± 2.9	**8h**	55.0 ± 2.4	**8r**	92.0 ± 4.1	**20e**	63.6 ± 14.9
3	66.2 ± 0.7	**8i**	84.8 ± 4.9	**8s**	80.9 ± 2.7	**20f**	74.7 ± 1.4
4	n.d.	**8j**	82.2 ± 1.3	**12a**	86.0 ± 3.2	**20g**	65.4 ± 2.9
8a	90.4 ± 1.7	**8k**	78.3 ± 2.6	**12b**	73.2 ± 4.1		
8b	68.1 ± 1.2	**8l**	n.d.	**12c**	83.8 ± 5.7		
8c	95.3 ± 2.7	**8m**	87.4 ± 3.4	**12d**	79.7 ± 7.4		
8d	82.9 ± 3.4	**8n**	n.d.	**20a**	69.1 ± 1.1		
8e	65.7 ± 3.6	**8o**	86.9 ± 6.3	**20b**	62.8 ± 8.4		
8f	78.9 ± 3.89	**8p**	77.0 ± 3.9	**20c**	77.6 ± 14.4		
8**g**	77.3 ± 0.3	**8q**	89.9 ± 3.0	**20d**	70.1 ± 6.7		

* Viability of cells in presence of 50 μM compound in comparison to an untreated sample. As positive control daunorubicin was used and an IC_{50} value of 12.55 ± 0.07 μM was determined.

n.d. not determined

CYTOTOXICITY ASSAY

The cytotoxicity of the compounds was tested against a human embryonic kidney cell line (HEK293). The cells were incubated with the compounds at a concentration of 50 μM for 45 h, and the cell viability was determined using the Alamar Blue assay. All tested compounds showed only a relatively weak cytotoxicity at the used concentration (Table 5).

CELLULAR ACTIVITY

To show cellular target engagement and selectivity, Western blotting experiments were performed with a selection of compounds in neuroblastoma BE(2)-C cells. The tumor cells were incubated for 6 h with 10 μM of compound **3, 8a, 8b, 8f** or **20a.** Cell lysates were blotted against Ac-SMC3 (HDAC8 substrate), Ac-α-tubulin (HDAC6 substrate) and Ac-histone H3 (HDAC1 substrate). As shown in Figure 6A, all compounds induced increase of both SMC3 and tubulin acetylation compared to solvent (DMSO) control, thus they inhibit both HDAC6 and HDAC8 in BE(2)-C cells. In contrast, no significant effect on the acetylation level of histone H3 was observed. This indicates that the observed in vitro selectivity is also detected in a cellular setting. A summary and quantification of all Western Blot repetitions is displayed in the corresponding bar diagram (Figure 6B).

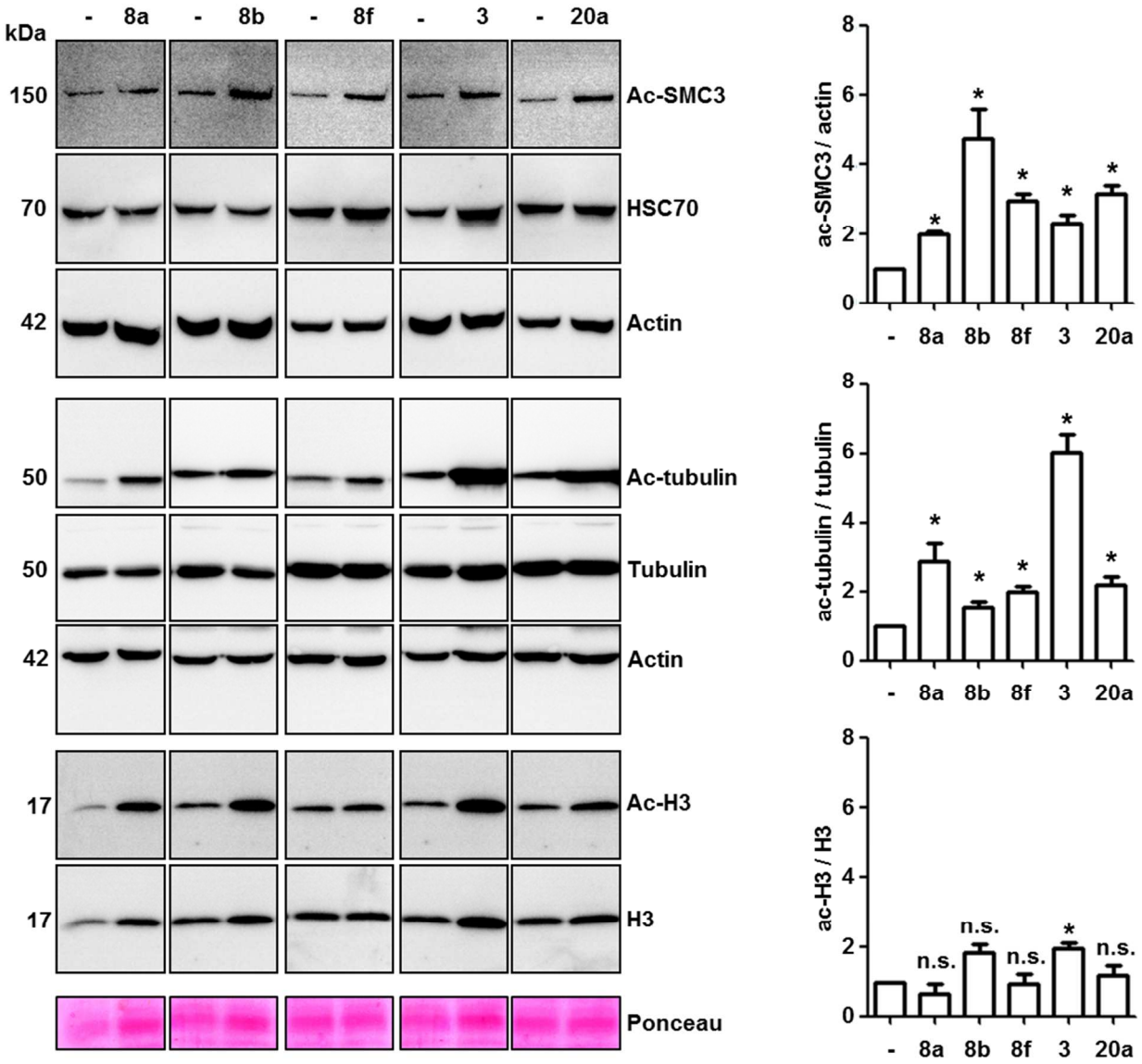

Figure 6. Cellular target engagement and selectivity. (**A**) Acetylation of SMC3, α-tubulin and histone H3 is shown in Western blots of whole-cell lysates 6 h after treatment of BE(2)-C cells with 10 μM of compound **3, 8a, 8b, 8f** or **20a.** HSC70, tubulin, histone H3, β-Actin and Ponceau staining were used as a loading control. (**B**) The normalized ratios from three independent experiments are shown in the bar graphs on the right.

Anti-neuroblastoma phenotype

In order to measure the functional consequence of HDAC8 inhibition, the BE(2)-C neuroblastoma cell model was applied, which responds with growth arrest and signs of neuronal differentiation upon knockdown or selective inhibition of HDAC8.[26] Growth arrest was determined by colony formation and viability assays. The induction of a more differentiated phenotype was detected by analysis of marker gene expression (*CDKN1A*, *TH* and *NTRK1*).

Tyrosine hydroxylase (TH) and neurotrophin receptor kinase A (*NTRK1/TrkA*) are neuronal marker genes. Tyrosine hydroxylase is encoded by the *TH* gene and is present in the central nervous system (CNS), peripheral sympathetic neurons and the adrenal medulla. The enzyme catalyzes the rate limiting step in this synthesis of catecholamines. Differentiation of neuroblastoma cells is accompanied by an increase in tyrosine hydroxylase (TH) mRNA.[50] Activation of the neurotrophin receptor TrkA signaling pathway leads to neuronal differentiation and high expression of NTRK1/TrkA is present in neuroblastomas with favorable biological features and is highly correlated with patient survival.[51] Differentiation is typically associated with a cell cycle arrest and CDK inhibitor $p21^{WAF1/CIP1}$ (*CDKN1A*) is known to mediate cell cycle arrest in response to pharmacological HDAC inhibition.

For colony formation assays, BE(2)-C cells were treated with 10 μM of each of the selected compound (**3, 8a, 8b, 8f, 20a**) for 96 h, followed by culturing for another 6 days without treatment. This assesses whether the treatment impairs the clonogenic growth capacity of tumor cells, indicating effectiveness of compounds on the survival and proliferation of tumor cells. All compounds significantly decreased the ability to form colonies (Figure 7A). The WST-8 metabolic activity assay was applied to determine metabolic IC_{50} values in BE(2)-C cells, employing six different inhibitor concentrations per compound and six replicates per inhibitor concentration.

The assay is based on the extracellular reduction of WST-8 by NADH produced in the mitochondria resulting in a water-soluble formazan which dissolves directly into the culture medium. It allows the colorimetric analysis of the number of viable cells. A reduction in cell viability or slowed-down proliferation results in lower metabolic activity. Thus, the metabolic IC_{50} value serves to determine growth arrest/cytotoxicity upon treatment with selected compounds compared to solvent treated control cells.

Two representative compounds, the 3-amino-4-methoxybenzhydroxamic acid **8b** and the 3-benzyloxy-4-methoxybenzhydroxamic acid **20a**, were chosen for this assay and compared with **1** (Figure 7B). In addition the upregulation of differentiation marker genes, such as *p21/CDKN1*, *TrkA/NTRK1* and *TH* was studied (Figure 7C). The developed inhibitors **8b** and **20a** showed a stronger upregulation compared to the reference inhibitor **1** and the outgrowth of neurofilament positive neurite-like structures (Figure 7D), indicating a strong HDAC8 inhibition phenotype.

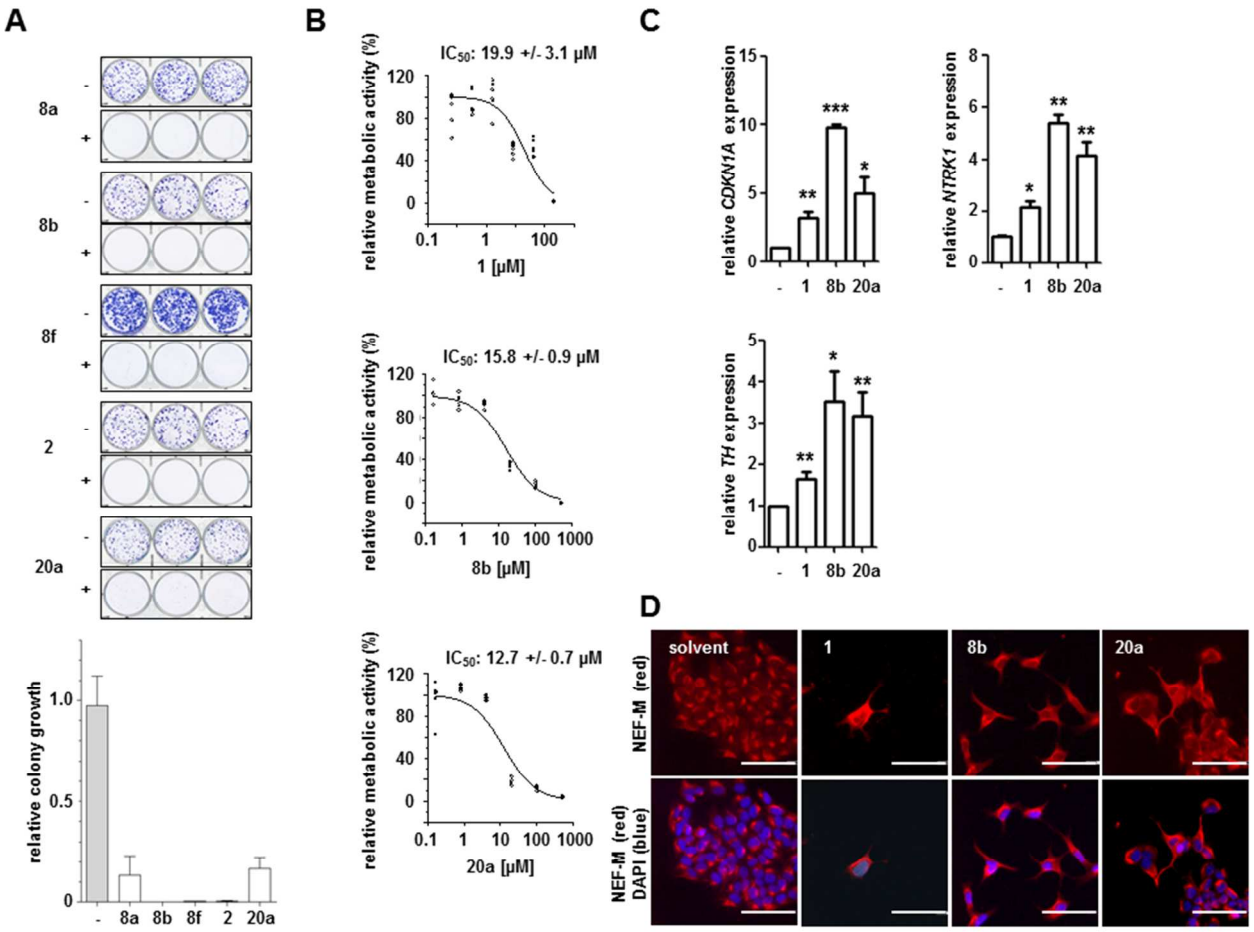

Figure 7. The developed HDAC inhibitors decrease clonogenic growth capacity as well as metabolic activity and induce signs of neuronal differentiation in BE(2)-C neuroblastoma cells. (A) Colonies were stained (pictures) and quantified (bar diagram). Where treatment is indicated, cells were treated with 10 µM compound for 96 h and colonies were stained after another 6 d of growth time. Solvent (DMSO) treatment is marked with a minus sign. **(B)** Displayed are the IC_{50} curves and the calculated metabolic IC_{50} values. After 24 h of culture, BE(2)-C cells were treated with the compounds for 72 h. After incubation with WST-8, fluorescence intensity was measured to determine the metabolic activity of the treated cells. **(C)** Realtime PCR was used to analyze the expression of differentiation markers (*CDKN1A, TH, NTRK1*). After 24 h of culture, BE(2)-C cells were treated with compounds (6 µM **1**; 10 µM **8b**; 10 µM **20a**) for 72 h. Expression was normalized to solvent (DMSO; marked with a minus sign)

treated cells. (**D**) Immunofluorescent pictures show neurofilament (red) and DAPI (blue) staining of BE(2)-C cells 6 days after treatment with 6 μM **1**; 10 μM **8b**; 10 μM **20a** (scale bar=100 μm).

CONCLUSIONS

Structure guided optimization of benzhydroxamic acids led to highly potent and selective HDAC8 inhibitors. Detailed structure-activity relationships were derived for the three series of synthesized inhibitors. The most selective inhibitor in vitro, the 3-benzylamino-benzhydroxamic acid **8f**, showed a 534/411 fold selectivity against HDAC1 and HDAC6, respectively. In the cellular testing, the 3-benzylamino-benzhydroxamic acid derivatives **8a**, **8b**, **8f** and the 3-benzyloxy-benzhydroxamic acid derivative **20a** showed cellular target engagement and did not increase histone acetylation. Phenotypic markers, which are characteristic for HDAC8 inhibition, are similarly detected upon treatment with the inhibitors, such as **8b** and **20a**. The phenotypic markers (e.g. p21/*CDKN1* upregulation, NEF staining and impaired colony formation ability) are the result of growth arrest and differentiation into a neuronal phenotype. The anti-neuroblastoma effects of the developed HDAC8 inhibitors **8b** and **20a** are at least as effective as those observed with **1**. These results suggest improved potential of selective HDAC inhibitors to target neuroblastoma without undesired side effects in vivo.

EXPERIMENTAL

Synthesis and analytics

Characterization data of the hydroxamic acids are listed in the Supporting Information.

All materials and reagents were purchased from Sigma–Aldrich Co. Ltd. and Carbolution Chemicals. All solvents were analytically pure and dried before use. Thin layer chromatography was carried out on aluminum sheets coated with silica gel 60 F254 (Merck, Darmstadt, Germany). For column chromatography under normal pressure silica gel 60 (0.036–0.200mm) was used.

Final compounds were confirmed to be of >95% purity based on HPLC. Purity was measured by UV absorbance at 256 nm. The HPLC consists of an XTerra RP18 column (3.5 µm 3.9 x 100 mm) from the manufacturer Waters (Milford, MA, USA), two LC-10AD pumps, a SPD-M10A VP PDA detector, and a SIL-HT auto sampler, all from the manufacturer Shimadzu (Kyoto, Japan). For preparative tasks a XTerra RP18 column (7 µm 19 x 150 mm) from the manufacturer Waters (Milford, MA, USA) and two LC-20AD pumps were used. The mobile phase was in all cases a gradient of methanol/water (starting at 95% water going to 5% water).

Mass spectrometry analyses were performed with a Finnigan MAT 710C (Thermo separation Products, San Jose, USA) for the ESI-MS spectra, and with a LTQ (linear ion trap)-Orbitrap XL hybrid mass spectrometer (Thermo Fisher Scientific, Bremen, Germany) for the HRMS-ESI (high resolution mass spectrometry) spectra. For the HRMS analyses the signal for the isotopes with the highest prevalence was given and calculated (^{35}Clor, ^{79}Brom).

^{1}H NMR and ^{13}C NMR spectra were taken on a Varian Gemini 2000 and a Varian Inova 500 using deuterated chloroform and deuterated DMSO as solvent. Chemical shifts are referenced to the residual solvent signals.

Procedure A. Synthetic procedures for the synthesis of the 3-(*N*-arylamino)benzhydroxamic acid derivatives (8a-s).

Synthesis of *N*-substituted-3-aminobenzoic acid derivatives (6a-k, 6m-q). The appropriate 4-substituted-3-aminobenzoic acid derivative (**5**; 2 mmol) was dissolved in toluene (100 mL), the respective aldehyde (4 mmol) was added and the reaction mixture was heated for 2 h under reflux using a water trap. Subsequently, the solvent was evaporated under reduced pressure. The crude product was dissolved in tetrahydrofuran and cooled to 0 °C, then sodium triacetoxyborohydride (16 mmol) was added and the reaction mixture was stirred for 15 min, after which acetic acid was given to the reaction and stirring was continued overnight at room temperature.[52] The reaction was quenched by adding water, and the pH was adjusted to 5 with aq. potassium hydrogen carbonate solution. The mixture was extracted with ethyl acetate (3 x 25 mL), and the organic layers were combined and evaporated under vacuum.For compound (**6k**), 4-chloroacetophenone was used instead of the aldehyde derivative.

Synthesis of 4-Methyl-3-[*N*-(2-phenylethyl)amino]benzoic acid (6l). Methyl 3-amino-4-methylbenzoic acid (1 mmol) was dissolved in 10 mL MeCN then phenethyl bromide (3 mmol) was added. The reaction was irradiated at 110° C for 10 min with 5 min warming time to 110°C in a microwave. After that, the solvent was removed and the mixture was purified by column chromatography (chloroform/ methanol, 98:2). In the next step, the ester was hydrolyzed using 1 M sodium hydroxide solution (10 mL) in methanol (40 mL). The reaction was refluxed for 1 h, after that methanol was removed under reduced pressure and the mixture was extracted with ethyl acetate (100 mL) and 1M hydrochloric acid solution (100 mL), the organic layers were combined and evaporated under vacuum to obtain the pure product.

Synthesis of 4-Methoxy-3-[*N*-(2-phenylethyl)amino]benzoic acid (6r) and 4-Methyl-3-[*N*-(3-phenylpropyl)-amino]benzoic acid (6s). The procedure described above for (**6l**) was used with

modified parameters for the microwave irradiation and for the purification of the final step. For (**6r**) and (**6s**), the microwave was set to 150 °C for 30 min with 5 min warming time. In addition, the final product was purified via preparative HPLC.

Boc-protection of 3-(*N*-Benzylamino)-4-methoxy- (6a) and 3-(*N*-Benzylamino)-4-methylbenzoic acid (6b). For compounds (**7a**) and (**7b**), the obtained crude amine (**6a** and **6b**, respectively) was dissolved in methanol (50 mL) and *tert*-butanol (50 mL), then Boc_2O was added and the reaction was stirred at room temperature overnight. The product was purified by column chromatography (chloroform/ methanol, 98:2).

Synthesis of the 3-(*N*-arylamino)benzhydroxamic acid derivatives (8a-s). The substituted benzoic acid derivative (1 eq.) was dissolved in dry tetrahydrofuran (50 mL), followed by the addition of PyBOP (1.2 eq.), and the mixture was stirred at room temperature for 15 min. To the activated acid a mixture of H_2NOTHP (1.5 eq.) and DIPEA (2.5 eq.) in dry tetrahydrofuran (5 mL) was added, and the reaction mixture was stirred at room temperature overnight.[40] For the 3-amino derivatives **(8a-s)**, the order of addition and also the amount of the reagents were changed to prevent side products. At first, the 3-aminobenzoic acid derivatives (**7a-s)** were dissolved in tetrahydrofuran followed by the addition of DIPEA and H_2NOTHP, and then PyBOP was added. The reaction was monitored by TLC, and the solvent was finally evaporated under vacuum and the residue was dissolved in ethyl acetate (50 mL) and washed with aq. potassium hydrogen carbonate solution and brine. The organic layer was evaporated under vacuum and the product was purified by column chromatography (chloroform/methanol/ TEA, 99.5:0.45:0.05).

The obtained product was dissolved in tetrahydrofuran, a catalytic amount of diluted hydrochloric acid was added, and the reaction mixture was stirred at room temperature. The reaction was controlled by TLC. Finally, the solvent was evaporated under vacuum, and the obtained

hydroxamic acid derivative was purified by column chromatography (chloroform/ methanol/ formic acid, 95:4.95:0.05).

In the case of **8a** and **8b**, the boc-protected hydroxamic acid derivatives were dissolved in a mixture of $CHCl_3$ (80 mL) and TFA (20 mL) and stirring was continued for 1 h at room temperature.[53] After that the mixture was cooled to 0 °C and an aq. potassium carbonate solution was added to adjust the pH to 6-7. The reaction mixture was extracted with $CHCl_3$ (3 x 25 mL), the organic layers were combined and evaporated under vacuum. The product was purified by column chromatography (chloroform/ methanol/ formic acid, 95:4.95:0.05).

Procedure B. Synthetic procedures for the synthesis of the 3-Phenylcarbamoylbenzhydroxamic acid derivatives (12a-d).

Synthesis of 2-Methoxy-5-methoxycarbonylbenzoic acid (9b).[41] To a solution of methyl 3-formyl-4-methoxybenzoic acid (**15**; 2.4 mmol), sodium dihydrogen phosphate (2.4 mmol), 2-methyl-2-butene (10.6 mmol) in *tert*-butanol and water was added sodium chlorite (8.17 mmol) and the mixture was stirred for 1 h at room temperature. The reaction mixture was adjusted to pH 4 by addition of 1 M hydrochloric acid. The aqueous layer was extracted with dichloromethane. The organic layers were combined, washed with brine, dried over anhydrous sodium sulfate, and concentrated under vacuum to give a white powder. Yield 60%, MS m/z: 209.23 $[M-H]^-$.

Synthesis of 2-Chloro-5-methoxycarbonylbenzoic acid (9c).[54] Methyl 4-chloro-3-formylbenzoic acid (**17**; 1 mmol) was dissolved in a mixture of acetone and water (1:1), followed by the addition of potassium permanganate (4 mmol). The solution was then stirred at room temperature for 4 h. 1 M sodium carbonate solution was added and the mixture was stirred for another 15 min. The mixture was then filtered and the pH of the filtrate was adjusted to 2-3 with

1 M hydrochloric acid. The formed precipitate was filtered, washed with water and dried to afford a white solid. Yield 57%, MS m/z: 213.31 $[M-H]^-$.

Synthesis of 5-Methoxycarbonyl-2-methylbenzoic acid (9d).[55] Methyl 3-iodo-4-methylbenzoic acid (**18**; 40 mmol) was dissolved in dry tetrahydrofuran, and the mixture was stirred at -20 °C under argon. Isopropylmagnesium chloride (2 M in tetrahydrofuran; 44 mmol) was slowly added and the suspension was stirred for further 1 h at -20 °C. Dry ice (8 g) was then quickly added and the resulting solution was stirred for another 1 h at room temperature. The solvent was removed under reduced pressure and 1 M hydrochloric acid solution was added. The precipitated product was filtered, washed with water and air dried to afford a white solid. Yield 96%, MS m/z: 193.36 $[M-H]^-$.

Synthesis of 3-Phenylcarbamoylbenzoic acid (11a). 2-Methoxycarbonylbenzoic acid (**9a**; 2 mmol) was dissolved in an excess of aniline cooled to 0 C using an ice bath then thionyl chloride (12 mmol) was added and the reaction was heated under reflux for 1 h. After that, aniline and the remaining thionyl chloride were removed under reduced pressure. The mixture was dissolved in ethyl acetate (50 mL) and washed with aq. potassium hydrogen carbonate solution and brine. The organic layer was evaporated under vacuum and the obtained product was purified by column chromatography (chloroform/ methanol, 99:5). In the next step, the ester **10a** was hydrolyzed using 1 M sodium hydroxide solution (10 mL) in methanol (40 mL). The reaction was refluxed for 1 h, methanol was subsequently removed under reduced pressure, and the mixture was extracted with ethyl acetate (100 ml) and 1 M hydrochloric acid solution (100 mL). The organic layers were combined and evaporated under vacuum to obtain the pure product. Yield 9%

Synthesis of 3-[(4-Chlorophenyl)carbamoyl]-4-substituted-benzoic acids (11b-d). The appropriate 5-methoxycarbonyl-2-substituted-benzoic acids (**9b-d**; 3 mmol), DMF (one drop) and oxalyl chloride (4 mmol) were stirred in CH_2Cl_2 at room temperature for 3 h. The mixture was

then added dropwise to a solution of 4-chloroaniline (3 mmol) and DIPEA (8 mmol) in CH_2Cl_2, and stirring was continued for another 2 h at room temperature.[41] The reaction mixture was washed with a saturated aqueous solution of ammonium chloride and brine. The organic layer was dried over anhydrous sodium sulfate, filtered, and evaporated under vacuum. The obtained product was purified by column chromatography (chloroform/methanol, 99:1). Yields 80-86%.

In the next step, the esters **10b-d** were hydrolyzed using 1 M sodium hydroxide solution (10 mL) in methanol (40 mL). The reaction was refluxed for 1 h, then methanol was removed under reduced pressure and the mixture was extracted with ethyl acetate and 1 M hydrochloric acid solution. The organic layers were combined and evaporated under reduced pressure to obtain the pure product. Yields 50-70%.

Synthesis of the 3-Phenylcarbamoylbenzhydroxamic acid derivatives (12a-d). The benzoic acid derivatives (**11a-d**) were converted to the corresponding benzhydroxamic acids following the same procedure as described for **8a-s**.

Synthesis of Methyl-3-formyl-4-hydroxybenzoic acid (14).[41] To a solution of methyl 4-hydroxybenzoic acid (**13**; 20 mmol) and triethylamine (118 mmol) in 1,2-dichloroethane was added anhydrous magnesium chloride (100 mmol) and the mixture was stirred for 1 h at 40 °C. Paraformaldehyde (197 mmol) was then added and the reaction was stirred for further 3 h at 70 °C. The reaction was cooled, quenched with 1 M hydrochloric acid solution, and filtered. The organic layer was separated, washed with 1 M hydrochloric acid and brine, dried over anhydrous sodium sulfate, and concentrated under reduced pressure. The product was purified by column chromatography (petroleum ether/ ethyl acetate 94:6-92:8). Yield 30%, MS m/z: 181.00 $[M+H]^+$.

Synthesis of Methyl-3-formyl-4-methoxybenzoic acid (15).[41] To a suspension of methyl 3-formyl-4-hydroxybenzoic acid (**14**; 50 mmol) and potassium carbonate (60 mmol) in acetone was added dimethyl sulfate (62 mmol). The mixture was stirred for 2 h under reflux. After cooling,

the mixture was filtered and the residue was washed with acetone. The solvent was removed under reduced pressure. The residue was extracted with ethyl acetate and a saturated aqueous solution of sodium hydrogen carbonate. The organic layer was separated, washed with brine, dried over anhydrous sodium sulfate, and the solvent was removed under reduced pressure. The product was pure enough for the next step. Yield 85%, MS m/z: 195.00 $[M+H]^+$.

Synthesis of Methyl-4-chloro-3-formylbenzoic acid (17).[54] Methyl 4-chloro-3-methylbenzoic acid (**16**; 10 mmol) was dissolved in a mixture of glacial acetic acid (17 mL), acetic anhydride (16.5 mL) and sulfuric acid (2.5 ml) at 0 °C. Chromium trioxide (30 mmol) was then added in small portions. The mixture was stirred in ice bath for further 3 h, then poured into ice water and stirred vigorously for 30 min. The resulting precipitate was filtered and washed with water to afford a gray solid which was dissolved in a mixture of methanol (16 mL), water (16 ml) and sulfuric acid (0.4 mL) and refluxed for 1 h. The residue was added into water, and the aqueous layer was extracted with ethyl acetate. The organic layer was washed with water and brine, and dried over anhydrous sodium sulfate. The solvent was evaporated under reduced pressure to yield the product, which was purified by column chromatography (petroleum ether/ethyl acetate 93:7-90:10). Yield 57%, MS m/z: 213.36 $[M-H]^-$.

Procedure C. Synthetic procedures for the synthesis 3-Benzyloxybenzhydroxamic acid derivatives (20a-g).

Synthesis of the 3-Benzyloxybenzhydroxamic acid derivatives (20a-g). The benzoic acid derivatives (**11a-d**) were converted to the corresponding benzhydroxamic acids following the same procedure as described for **8a-s**.

Synthesis of Methyl-3-hydroxy-4-substituted-benzoic acid (22). The appropriate 3-hydroxy-4-substituted-benzoic acid (**21**; 0.87 mmol) was dissolved in 50 mL methanol and cooled to 0 °C. Then thionyl chloride (2.64 mmol) was added dropwise and the reaction mixture was heated for 5

h under reflux. Subsequently, the solvent was evaporated under reduced pressure. The crude product was dissolved in ethyl acetate and washed with aq. sodium hydroxide solution. The organic layer was dried over anhydrous sodium sulfate and concentrated under reduced pressure. The product was purified by column chromatography (chloroform methanol, 99:1). Yields 91-99%.

Methyl-3-(chloro-substituted-benzyloxy)-4-substituted-benzoates (24b-g). The appropriate methyl 3-hydroxy-4-substituted-benzoic acid (**22**; 1 mmol) was dissolved in 20 mL DMF and cooled to 0 °C, then potassium carbonate (3 mmol) and the appropriate chloro-substituted-benzyl bromide (**23**; 1.6 mmol) were added. The reaction mixture was stirred for 3 h at 80 °C. It was then diluted with brine and extracted with ethyl acetate. The organic layer was concentrated under reduced pressure and the product was purified by column chromatography (chloroform, 100). In the next step, the obtained esters (**24b-g**) were hydrolyzed using 1 M sodium hydroxide solution (10 mL) in methanol (40 mL) to get the carboxylic acid for the following synthesis of the corresponding hydroxamic acids **20b-g**. The reaction was refluxed for 3 h, then methanol was removed under reduced pressure and the mixture was extracted with ethyl acetate and 1 M hydrochloric acid solution. The organic layer was evaporated under reduced pressure and the crude product was purified by column chromatography (chloroform/ methanol, 97:3). Yields 69-81%.

Molecular docking

Ligand preparation.

MOE[56] (version 2014.09, Chemical Computing Group, Montreal, Canada) was used to generate the molecular structures of all compounds. The ligands were subsequently prepared for docking using the LigPrep tool[57] as implemented in Schrödinger's software, where all possible tautomeric forms as well as stereoisomers were generated and energy minimized using the OPLS force field.

Conformers of the prepared ligands were calculated with ConfGen using the default settings (Fast) and allowing minimization of the output conformations.

Protein preparation.

HDAC8: The crystal structure of HDAC8 in complex with a hydroxamic acid-based inhibitor (PDB ID: 2V5X) was retrieved from the Protein Data Bank (PDB; www.rcsb.org).[58] All water molecules were deleted except the two water molecules occupying the catalytic pocket HOH2061 and 2152, which were kept in the docking step. The protein structure was subsequently prepared with Schrödinger's Protein Preparation Wizard[59]: Hydrogen atoms were added and the H-bond network was subsequently optimized. The protonation states at pH 7.0 were predicted using the PROPKA tool in Schrödinger. The structures were finally subjected to a restrained energy minimization step using the OPLS2005 force field (RMSD of the atom displacement for terminating the minimization was 0.3 Å).

HDAC6: Docking studies in HDAC6 were performed in both the crystal structure of human HDAC6 in complex with trichostatin A (PDB ID: 5EDU) and zebrafish HDAC6 in complex with nexturastat A (PDB ID: 5G0I). Two reasons prompted us to dock in both orthologues. Indeed, the binding pockets in catalytic domain 2 (CD2) of both orthologues show a 100% sequence identity, nevertheless, water molecules in the catalytic pocket are absent in the only available crystal structure of hHDAC6 (PDB ID: 5EDU). Our docking studies have generally demonstrated the necessity of keeping the water molecule located at the rim of the catalytic tunnel (in the vicinity of His614; DrHDAC8) to improve the accuracy of the predicted binding mode. This water molecule is conserved in all reported crystal structures of DrHDAC6 as well as in crystal structures of homologous HDACs. Further, in the crystal structure of hHDAC6 trichostatin A chelates the zinc ion in a bidentate fashion. Meanwhile, nexturastat A which, similar to the herein

described compounds, possesses a benzhydroxamic acid head group shows only a mono-dentate chelation of the catalytic zinc ion of HDAC6 (PDB ID: 5G0I).

For docking, only CD2 of chain A of both PDB structures was kept. The proteins were subsequently prepared as described for HDAC8. The previously mentioned water molecule (HOH2249 in PDB ID 5G0I) was considered during the subsequent docking step.

HDAC1: The crystal structure of HDAC1 (PDB ID: 4BKX) was retrieved and prepared as previously described for HDAC8.

Docking.

The receptor grid preparation for the docking procedure was carried out by assigning the co-crystallized ligand as the centroid of the grid box. In the case of HDAC1, only residues Ala15-Arg17 of the peptide were considered as ligand for assigning the grid box. The generated 3D conformers were docked into the receptor model using Glide[60] (Schrödinger Inc., New York, USA) in the Standard Precision mode. A total of 20 poses per ligand conformer were included in the post-docking minimization step and a maximum of two docking poses were output for each ligand conformer.

PAINS filter. All the herein described benzhydroxamic acids were filtered for pan-assay interference compounds[61] (PAINS). For this purpose, PAINS1, PAINS2 and PAINS3 filters, as implemented in Schrödinger's Canvas program,[62] were employed. None of the compounds was flagged as PAINS.

In vitro testing

Recombinant human HDAC1 and -6 were purchased from BPS Biosciences. Enzyme inhibition was determined by using a homogenous fluorescence assay which was described before.[63]. The enzymes were incubated for 90 min at 37 °C, with the fluorogenic substrate ZMAL (Z-(Ac)Lys-

AMC) in a concentration of 10.5 μM and increasing concentrations of inhibitors. Fluorescence intensity was measured at an excitation wavelength of 390 nm and an emission wavelength of 460 nm in a microtiter plate reader (BMG Polarstar).

Recombinant hHDAC8 was produced as described before.[64] The HDAC8 activity assay was performed using a commercial HDAC8 Fluorimetric Drug Discovery Kit [Fluor de Lys(R)-HDAC8, BML-KI178] according to the manufacturer's instructions as described earlier[40]. The enzyme was incubated for 90 min at 37 °C, with a substrate concentration of 50 μM and increasing concentrations of inhibitors. Measurement was performed as described for HDAC1/6.

Cytotoxicity studies

HEK293 cells (DSMZ Braunschweig, ACC305) were incubated at 37 °C in a humidified incubator with 5% CO_2 in Dulbecco's Modified Eagle Medium (DMEM) supplemented with 10% FCS and 5 mM glutamine. Cells were seeded out at 1.5 x 10^3 cells per well in a 96-well cell culture plate (TPP, Switzerland). The compounds were added immediately to the medium at 50 μM or increasing concentrations to determine IC_{50} values. After 24 h, AlamarBlue reagent (Invitrogen, CA) was added according to the manufacturer's instructions and incubated again for 21 h before samples were analysed. Detection of viable cells which convert the resazurine compound of reagent into the high fluorescent resorufin was performed by using a FLUOstarOPTIMA microplate reader (BMG Labtec) with the following filter set: Ex 560 nm / Em 590 nm. All measurements were performed in triplicates and data are means with SD $\leq$ 12%. As a positive control daunorubicin was used and an IC_{50} value of 12.55 ± 0.07 μM was determined.

Cellular testing

Cell culture. Neuroblastoma BE(2)-C (ECACC, Salisbury, UK) cells were grown under standard conditions in DMEM with l-glutamine, 4.5 g/l glucose (Lonza, Basel, Switzerland) and 1% non-essential amino acids (NEAA) (Invitrogen, Darmstadt, Germany), supplemented with 10% fetal bovine serum (FBS) (Sigma, Munich, Germany). BE(2)-C cells were genotyped in April 2012 (DSMZ) and were routinely (once per month) tested for mycoplasma contamination.

Western Blot. Western blot analysis was performed as described previously.[26] (The following antibodies were used for detection: anti-acetyl-SMC3 (provided by Prof. K Shirahige, University of Tokyo, Tokyo, Japan), anti-acetyl tubulin (clone 6-11B-1; Sigma), anti-acetyl-histone H3 (polyclonal; Millipore, Schwalbach am Taunus, Germany), anti HSC70/HSP70 (polyclonal; Santa Cruz), anti-tubulin (polyclonal; Cell Signaling Technology, Leiden, Netherlands), anti-histone H3 (polyclonal; Cell Signaling Technology), anti-β-actin (clone AC-15; Sigma).

Colony Assay. In six-well plates, 500 cells were seeded and treated 18 to 24 hours after seeding as indicated. After 96 h of treatment, the medium was changed to fresh medium containing no compounds. After a minimum of another seven days, viable colonies were stained with crystal violet (1% in 70% ethanol). For quantification, the plates were scanned in and colonies were counted in 16-bit binary pictures with the ITCN plugin for ImageJ software (U. S. National Institutes of Health, Bethesda, MD, USA; http://imagej.nih.gov/ij/).

Cell-Viability. Metabolic activity was colorimetrically determined using the WST-8 assay (GERBU Biotechnik GmbH, Heidelberg, Germany) according to the manufacturer's instructions. Absorbance was quantified using the "FLUOstar OPTIMA" multiwell plate reader and IC_{50} values were calculated with GraphPad Prism version 5.00 for Windows (GraphPad Software, San Diego, CA, USA, www.graphpad.com).

Realtime PCR. Real-time reverse transcription–PCR was performed as described previously.[14] Data were normalized against neuroblastoma housekeeping genes *SDHA* and *HPRT*[65] and set in

relation to negative control. The following specific primer pairs were used: *CDKN1* (forward: 5'-TGG AGA CTC TCA GGG TCG AAA-3', reverse: 5'-GGC GTT TGG AGT GGT AGA AAT C-3'), *HPRT* (forward: 5'-TGA CAC TGG CAA AAC AAT GCA-3', reverse: 5'-GGT CCT TTT CAC CAG CAA GCT-3'), *NTRK1* (forward: 5'-CAG CCG GCA CCG TCT CT-3', reverse: 5'-TCC AGG AAC TCA GTG AAG ATG AAG-3'), *SDHA* (forward: 5'-TGG GAA CAA GAG GGC ATC TG-3', reverse: 5'-CCA CCA CTG CAT CAA ATT CAT G-3'). The *TH* prime pair was from Qiagen (QT00067221).

Immunofluorescence staining. BE(2)-C cells (3×10^4) were grown on 8-well chambers (ibidi). Six days after treatment with compounds, cells were fixed for 15 min in 2% (w/v) paraformaldehyde and permeabilized for 15 min with 0.1% (v/v) Triton X-100 in PBS. After washing thrice with PBS, cells were blocked [PBS-Triton with 10% goat serum and 0.25% (w/v) BSA] for 1h at room temperature, incubated overnight with anti-NEF-M antibody (polyclonal rabbit, Millipore; 1:500) at 4°C, washed with PBS, and incubated with Cy3-labeled goat anti-rabbit antibody (Dianova; 1:200) for 3 h at room temperature. Nuclei were co-stained with 250 ng/mL DAPI solution and analyzed with the Olympus CKX41 microscope and ColorView I FW camera.

ASSOCIATED CONTENT

Supporting Information. Spectral data for the compounds, docking figures, and molecular formula strings (CSV). This material is available free of charge.

AUTHOR INFORMATION

Corresponding Author

*Dr. Wolfgang Sippl, Institute of Pharmacy, Martin-Luther University of Halle-Wittenberg, 06120 Halle/Saale, Germany. Tel. +493455525040. E-mail: wolfgang.sippl@pharmazie.uni-halle.de.

Author Contributions

The manuscript was written through contributions of all authors. All authors have given approval to the final version of the manuscript.

Funding Sources

This study was supported by the Deutsche Forschungsgemeinschaft (DFG, Ju 295/13-1, Si 846/13-1, Oe 542/2-1, Wi 1461-/4-1). FRK was supported by the Deutsche Krebshilfe (DKH) with a Mildred Scheel doctoral scholarship (number 112065).

ABBREVIATIONS

AcOH, acetic acid; Ac_2O, acetic anhydride; aq., aqueous; Boc, *tert*-butyloxycarbonyl; Boc_2O, di-tert-butyl dicarbonate; DAPI, 4′,6-Diamidin-2-phenylindol; DIPEA, di-isopropyl ethylamine; DMF, *N*,*N*-dimethylformamide; (d)DMSO, (deuterated) dimethyl sulfoxide; EDC, ethylene dichloride; EtOAc, ethyl acetate; eq., equivalent; *i*-PrMgCl, iso propyl magnesium chloride; MeCN, acetonitrile; MeOH, methanol; $Na(AcO)_3BH$,sodium triacetoxy borohydride; n.a., not active; n.d., not determined; NEF, negative factor; H_2NOTHP, *O*-(tetrahydro-2*H*-pyran-2-yl)hydroxylamine; PCR, polymerase chain reaction; PBS, phosphate-buffered saline; PyBOP, benzotriazol-1-yl-oxytripyrrolidinophosphonium hexafluorophosphate; sol., solution; t-BuOH, *tert*-butanol; TEA, triethylamine; TFA, trifluoracetic acid; THF, tetrahydrofuran; TLC, thin layer chromatography; vdW, van-der-Waals.

REFERENCES

1. Matthay, K. K.; Maris, J. M.; Schleiermacher, G.; Nakagawara, A.; Mackall, C. L.; Diller, L.; Weiss, W. A. Neuroblastoma. *Nat. Rev. Dis. Primers* **2016**, *2*, 16078.

2. Applebaum, M. A.; Henderson, T. O.; Lee, S. M.; Pinto, N.; Volchenboum, S. L.; Cohn, S. L. Second malignancies in patients with neuroblastoma: the effects of risk-based therapy. *Pediatr. Blood Cancer* **2015**, *62*, 128-133.

3. Brodeur, G. M.; Iyer, R.; Croucher, J. L.; Zhuang, T. G.; Higashi, M.; Kolla, V. Therapeutic targets for neuroblastomas. *Expert Opin. Ther. Targets* **2014**, *18*, 277-292.

4. Schwab, M.; Alitalo, K.; Klempnauer, K. H.; Varmus, H. E.; Bishop, J. M.; Gilbert, F.; Brodeur, G.; Goldstein, M.; Trent, J. Amplified DNA with limited homology to myc cellular oncogene is shared by human neuroblastoma cell lines and a neuroblastoma tumour. *Nature* **1983**, *305*, 245-248.

5. Schwab, M.; Varmus, H. E.; Bishop, J. M. Human N-myc gene contributes to neoplastic transformation of mammalian cells in culture. *Nature* **1985**, *316*, 160-162.

6. Schwab, M.; Varmus, H. E.; Bishop, J. M.; Grzeschik, K. H.; Naylor, S. L.; Sakaguchi, A. Y.; Brodeur, G.; Trent, J. Chromosome localization in normal human cells and neuroblastomas of a gene related to c-myc. *Nature* **1984**, *308*, 288-291.

7. Brodeur, G. M.; Seeger, R. C.; Schwab, M.; Varmus, H. E.; Bishop, J. M. Amplification of N-myc in untreated human neuroblastomas correlates with advanced disease stage. *Science* **1984**, *224*, 1121-1124.

8. Mosse, Y. P.; Laudenslager, M.; Longo, L.; Cole, K. A.; Wood, A.; Attiyeh, E. F.; Laquaglia, M. J.; Sennett, R.; Lynch, J. E.; Perri, P.; Laureys, G.; Speleman, F.; Kim, C.; Hou, C.; Hakonarson, H.; Torkamani, A.; Schork, N. J.; Brodeur, G. M.; Tonini, G. P.; Rappaport, E.;

Devoto, M.; Maris, J. M. Identification of ALK as a major familial neuroblastoma predisposition gene. *Nature* **2008**, *455*, 930-935.

9. Ardini, E.; Magnaghi, P.; Orsini, P.; Galvani, A.; Menichincheri, M. Anaplastic Lymphoma Kinase: role in specific tumours, and development of small molecule inhibitors for cancer therapy. *Cancer Lett.* **2010**, *299*, 81-94.

10. Maris, J. M.; Hogarty, M. D.; Bagatell, R.; Cohn, S. L. Neuroblastoma. *Lancet* **2007**, *369*, 2106-2120.

11. Marks, P. A. The clinical development of histone deacetylase inhibitors as targeted anticancer drugs. *Expert Opin. Invest. Drugs* **2010**, *19*, 1049-1066.

12. Bolden, J. E.; Peart, M. J.; Johnstone, R. W. Anticancer activities of histone deacetylase inhibitors. *Nat. Rev. Drug Discovery* **2006**, *5*, 769-784.

13. Wagner, J. M.; Hackanson, B.; Lubbert, M.; Jung, M. Histone deacetylase (HDAC) inhibitors in recent clinical trials for cancer therapy. *Clin. Epigenet.* **2010**, *1*, 117-136.

14. Oehme, I.; Deubzer, H. E.; Wegener, D.; Pickert, D.; Linke, J. P.; Hero, B.; Kopp-Schneider, A.; Westermann, F.; Ulrich, S. M.; von Deimling, A.; Fischer, M.; Witt, O. Histone deacetylase 8 in neuroblastoma tumorigenesis. *Clin. Cancer Res.* **2009**, *15*, 91-99.

15. Waltregny, D.; De Leval, L.; Glenisson, W.; Ly Tran, S.; North, B. J.; Bellahcene, A.; Weidle, U.; Verdin, E.; Castronovo, V. Expression of histone deacetylase 8, a class I histone deacetylase, is restricted to cells showing smooth muscle differentiation in normal human tissues. *Am. J. Pathol.* **2004**, *165*, 553-564.

16. Waltregny, D.; Glenisson, W.; Tran, S. L.; North, B. J.; Verdin, E.; Colige, A.; Castronovo, V. Histone deacetylase HDAC8 associates with smooth muscle alpha-actin and is essential for smooth muscle cell contractility. *FASEB J.* **2005**, *19*, 966-968.

17. Chakrabarti, A.; Oehme, I.; Witt, O.; Oliveira, G.; Sippl, W.; Romier, C.; Pierce, R. J.; Jung, M. HDAC8: a multifaceted target for therapeutic interventions. *Trends Pharmacol. Sci.* **2015**, *36*, 481-492.

18. Zhang, K.; Lu, Y.; Jiang, C.; Liu, W.; Shu, J.; Chen, X.; Shi, Y.; Wang, E.; Wang, L.; Hu, Q.; Dai, Y.; Xiong, B. HDAC8 functions in spindle assembly during mouse oocyte meiosis. *Oncotarget* **2017**, *8*, 20092-20102.

19. Ahn, M. Y.; Yoon, J. H. Histone deacetylase 8 as a novel therapeutic target in oral squamous cell carcinoma. *Oncol. Rep.* **2017**, *37*, 540-546.

20. Deardorff, M. A.; Bando, M.; Nakato, R.; Watrin, E.; Itoh, T.; Minamino, M.; Saitoh, K.; Komata, M.; Katou, Y.; Clark, D.; Cole, K. E.; De Baere, E.; Decroos, C.; Di Donato, N.; Ernst, S.; Francey, L. J.; Gyftodimou, Y.; Hirashima, K.; Hullings, M.; Ishikawa, Y.; Jaulin, C.; Kaur, M.; Kiyono, T.; Lombardi, P. M.; Magnaghi-Jaulin, L.; Mortier, G. R.; Nozaki, N.; Petersen, M. B.; Seimiya, H.; Siu, V. M.; Suzuki, Y.; Takagaki, K.; Wilde, J. J.; Willems, P. J.; Prigent, C.; Gillessen-Kaesbach, G.; Christianson, D. W.; Kaiser, F. J.; Jackson, L. G.; Hirota, T.; Krantz, I. D.; Shirahige, K. HDAC8 mutations in Cornelia de Lange syndrome affect the cohesin acetylation cycle. *Nature* **2012**, *489*, 313-317.

21. Deardorff, M. A.; Porter, N. J.; Christianson, D. W. Structural aspects of HDAC8 mechanism and dysfunction in Cornelia de Lange syndrome spectrum disorders. *Protein Sci.* **2016**, *25*, 1965-1976.

22. Decroos, C.; Bowman, C. M.; Moser, J. A.; Christianson, K. E.; Deardorff, M. A.; Christianson, D. W. Compromised structure and function of HDAC8 mutants identified in Cornelia de Lange Syndrome spectrum disorders. *ACS Chem. Biol.* **2014**, *9*, 2157-2164.

23. Balasubramanian, S.; Ramos, J.; Luo, W.; Sirisawad, M.; Verner, E.; Buggy, J. J. A novel histone deacetylase 8 (HDAC8)-specific inhibitor PCI-34051 induces apoptosis in T-cell lymphomas. *Leukemia* **2008**, *22*, 1026-1034.

24. Zhao, G.; Wang, G.; Bai, H.; Li, T.; Gong, F.; Yang, H.; Wen, J.; Wang, W. Targeted inhibition of HDAC8 increases the doxorubicin sensitivity of neuroblastoma cells via up regulation of miR-137. *Eur. J. Pharmacol.* **2017**, *802*, 20-26.

25. Lopez, G.; Bill, K. L.; Bid, H. K.; Braggio, D.; Constantino, D.; Prudner, B.; Zewdu, A.; Batte, K.; Lev, D.; Pollock, R. E. HDAC8, a potential therapeutic target for the treatment of malignant peripheral nerve sheath tumors (MPNST). *PLoS One* **2015**, *10*, e0133302.

26. Rettig, I.; Koeneke, E.; Trippel, F.; Mueller, W. C.; Burhenne, J.; Kopp-Schneider, A.; Fabian, J.; Schober, A.; Fernekorn, U.; von Deimling, A.; Deubzer, H. E.; Milde, T.; Witt, O.; Oehme, I. Selective inhibition of HDAC8 decreases neuroblastoma growth in vitro and in vivo and enhances retinoic acid-mediated differentiation. *Cell Death Dis.* **2015**, *6*, e1657.

27. Krennhrubec, K.; Marshall, B. L.; Hedglin, M.; Verdin, E.; Ulrich, S. M. Design and evaluation of 'Linkerless' hydroxamic acids as selective HDAC8 inhibitors. *Bioorg. Med. Chem. Lett.* **2007**, *17*, 2874-2878.

28. Hu, E.; Dul, E.; Sung, C. M.; Chen, Z.; Kirkpatrick, R.; Zhang, G. F.; Johanson, K.; Liu, R.; Lago, A.; Hofmann, G.; Macarron, R.; de los Frailes, M.; Perez, P.; Krawiec, J.; Winkler, J.; Jaye, M. Identification of novel isoform-selective inhibitors within class I histone deacetylases. *J. Pharmacol. Exp. Ther.* **2003**, *307*, 720-728.

29. Chakrabarti, A.; Melesina, J.; Kolbinger, F. R.; Oehme, I.; Senger, J.; Witt, O.; Sippl, W.; Jung, M. Targeting histone deacetylase 8 as a therapeutic approach to cancer and neurodegenerative diseases. *Future Med. Chem.* **2016**, *8*, 1609-1634.

30. Suzuki, T.; Ota, Y.; Ri, M.; Bando, M.; Gotoh, A.; Itoh, Y.; Tsumoto, H.; Tatum, P. R.; Mizukami, T.; Nakagawa, H.; Iida, S.; Ueda, R.; Shirahige, K.; Miyata, N. Rapid discovery of highly potent and selective inhibitors of histone deacetylase 8 using click chemistry to generate candidate libraries. *J. Med. Chem.* **2012**, *55*, 9562-9575.

31. Suzuki, T.; Muto, N.; Bando, M.; Itoh, Y.; Masaki, A.; Ri, M.; Ota, Y.; Nakagawa, H.; Iida, S.; Shirahige, K.; Miyata, N. Design, synthesis, and biological activity of NCC149 derivatives as histone deacetylase 8-selective inhibitors. *ChemMedChem* **2014**, *9*, 657-664.

32. Huang, W. J.; Wang, Y. C.; Chao, S. W.; Yang, C. Y.; Chen, L. C.; Lin, M. H.; Hou, W. C.; Chen, M. Y.; Lee, T. L.; Yang, P.; Chang, C. I. Synthesis and biological evaluation of ortho-aryl *N*-hydroxycinnamides as potent histone deacetylase (HDAC) 8 isoform-selective inhibitors. *ChemMedChem* **2012**, *7*, 1815-1824.

33. Tang, W.; Luo, T.; Greenberg, E. F.; Bradner, J. E.; Schreiber, S. L. Discovery of histone deacetylase 8 selective inhibitors. *Bioorg. Med. Chem. Lett.* **2011**, *21*, 2601-2605.

34. Ingham, O. J.; Paranal, R. M.; Smith, W. B.; Escobar, R. A.; Yueh, H.; Snyder, T.; Porco, J. A., Jr.; Bradner, J. E.; Beeler, A. B. Development of a potent and selective HDAC8 inhibitor. *ACS Med. Chem. Lett.* **2016**, *7*, 929-932.

35. Whitehead, L.; Dobler, M. R.; Radetich, B.; Zhu, Y.; Atadja, P. W.; Claiborne, T.; Grob, J. E.; McRiner, A.; Pancost, M. R.; Patnaik, A.; Shao, W.; Shultz, M.; Tichkule, R.; Tommasi, R. A.; Vash, B.; Wang, P.; Stams, T. Human HDAC isoform selectivity achieved via exploitation of the acetate release channel with structurally unique small molecule inhibitors. *Bioorg. Med. Chem.* **2011**, *19*, 4626-4634.

36. Galletti, P.; Quintavalla, A.; Ventrici, C.; Giannini, G.; Cabri, W.; Penco, S.; Gallo, G.; Vincenti, S.; Giacomini, D. Azetidinones as zinc-binding groups to design selective HDAC8 inhibitors. *ChemMedChem* **2009**, *4*, 1991-2001.

37. Ononye, S. N.; VanHeyst, M. D.; Oblak, E. Z.; Zhou, W.; Ammar, M.; Anderson, A. C.; Wright, D. L. Tropolones as lead-like natural products: the development of potent and selective histone deacetylase inhibitors. *ACS Med. Chem. Lett.* **2013**, *4*, 757-761.

38. De Vreese, R.; D'hooghe, M. Synthesis and applications of benzohydroxamic acid-based histone deacetylase inhibitors. *Eur. J. Med. Chem.* **2017**, *135*, 174-195.

39. Di Micco, S.; Chini, M. G.; Terracciano, S.; Bruno, I.; Riccio, R.; Bifulco, G. Structural basis for the design and synthesis of selective HDAC inhibitors. *Bioorg. Med. Chem.* **2013**, *21*, 3795-3807.

40. Heimburg, T.; Chakrabarti, A.; Lancelot, J.; Marek, M.; Melesina, J.; Hauser, A. T.; Shaik, T. B.; Duclaud, S.; Robaa, D.; Erdmann, F.; Schmidt, M.; Romier, C.; Pierce, R. J.; Jung, M.; Sippl, W. Structure-based design and synthesis of novel inhibitors targeting HDAC8 from Schistosoma mansoni for the treatment of schistosomiasis. *J. Med. Chem.* **2016**, *59*, 2423-2435.

41. Hada, K.; Suda, A.; Asoh, K.; Tsukuda, T.; Hasegawa, M.; Sato, Y.; Ogawa, K.; Kuramoto, S.; Aoki, Y.; Shimma, N.; Ishikawa, T.; Koyano, H. Angiogenesis inhibitors identified by cell-based high-throughput screening: synthesis, structure-activity relationships and biological evaluation of 3-[(E)-styryl]benzamides that specifically inhibit endothelial cell proliferation. *Bioorg. Med. Chem.* **2012**, *20*, 1442-1460.

42. Tasler, S.; Muller, O.; Wieber, T.; Herz, T.; Pegoraro, S.; Saeb, W.; Lang, M.; Krauss, R.; Totzke, F.; Zirrgiebel, U.; Ehlert, J. E.; Kubbutat, M. H.; Schachtele, C. Substituted 2-arylbenzothiazoles as kinase inhibitors: hit-to-lead optimization. *Bioorg. Med. Chem.* **2009**, *17*, 6728-6737.

43. Vannini, A.; Volpari, C.; Gallinari, P.; Jones, P.; Mattu, M.; Carfi, A.; De Francesco, R.; Steinkuhler, C.; Di Marco, S. Substrate binding to histone deacetylases as shown by the crystal structure of the HDAC8-substrate complex. *EMBO Rep.* **2007**, *8*, 879-884.

44. Millard, C. J.; Watson, P. J.; Celardo, I.; Gordiyenko, Y.; Cowley, S. M.; Robinson, C. V.; Fairall, L.; Schwabe, J. W. Class I HDACs share a common mechanism of regulation by inositol phosphates. *Mol. Cell* **2013**, *51*, 57-67.

45. Hai, Y.; Christianson, D. W. Histone deacetylase 6 structure and molecular basis of catalysis and inhibition. *Nat. Chem. Biol.* **2016**, *12*, 741-747.

46. Miyake, Y.; Keusch, J. J.; Wang, L.; Saito, M.; Hess, D.; Wang, X.; Melancon, B. J.; Helquist, P.; Gut, H.; Matthias, P. Structural insights into HDAC6 tubulin deacetylation and its selective inhibition. *Nat. Chem. Biol.* **2016**, *12*, 748-754.

47. Rodrigues, D. A.; Ferreira-Silva, G. A.; Ferreira, A. C.; Fernandes, R. A.; Kwee, J. K.; Sant'Anna, C. M.; Ionta, M.; Fraga, C. A. Design, synthesis, and pharmacological evaluation of novel *N*-acylhydrazone derivatives as potent histone deacetylase 6/8 dual inhibitors. *J. Med. Chem.* **2016**, *59*, 655-670.

48. Wang, L.; Kofler, M.; Brosch, G.; Melesina, J.; Sippl, W.; Martinez, E. D.; Easmon, J. 2-Benzazolyl-4-piperazin-1-ylsulfonylbenzenecarbohydroxamic acids as novel selective histone deacetylase-6 inhibitors with antiproliferative activity. *PLoS One* **2015**, *10*, e0134556.

49. Olson, D. E.; Wagner, F. F.; Kaya, T.; Gale, J. P.; Aidoud, N.; Davoine, E. L.; Lazzaro, F.; Weiwer, M.; Zhang, Y. L.; Holson, E. B. Discovery of the first histone deacetylase 6/8 dual inhibitors. *J. Med. Chem.* **2013**, *56*, 4816-4820.

50. Summerhill, E. M.; Wood, K.; Fishman, M. C. Regulation of tyrosine hydroxylase gene expression during differentiation of neuroblastoma cells. *Brain Res.* **1987**, *388*, 99-103.

51. Eggert, A.; Ikegaki, N.; Liu, X.; Chou, T. T.; Lee, V. M.; Trojanowski, J. Q.; Brodeur, G. M. Molecular dissection of TrkA signal transduction pathways mediating differentiation in human neuroblastoma cells. *Oncogene* **2000**, *19*, 2043-2051.

52. Abdel-Magid, A. F.; Mehrman, S. J. A review on the use of sodium triacetoxyborohydride in the reductive amination of ketones and aldehydes. *Organic Process Research & Development* **2006**, *10*(5), 971-1031.

53. Kocienski, P. J. Protecting Groups, 3rd ed.: Georg Thieme Verlag: New York, **2005,** p 206.

54. Jiao, Y.; Xin, B. T.; Zhang, Y.; Wu, J.; Lu, X.; Zheng, Y.; Tang, W.; Zhou, X. Design, synthesis and evaluation of novel 2-(1*H*-imidazol-2-yl) pyridine sorafenib derivatives as potential BRAF inhibitors and anti-tumor agents. *Eur. J. Med. Chem.* **2015**, *90*, 170-183.

55. Meca, L.; Císařová, I.; Drahoňovský, D.; Dvořák, D. Enantiomerically pure axially chiral aminocarbene complexes of chromium. *Organometallics* **2008**, *27*(8), 1850-1858.

56. *Molecular Operating Environment (MOE)*, 2014.09; Chemical Computing Group Inc., 1010 Sherbooke St. West, Suite #910, Montreal, QC, Canada, H3A 2R7, 2014.

57. *Schrödinger Release 2014-2*: LigPrep, Schrödinger, LLC, New York, NY, 2014.

58. Berman, H. M.; Westbrook, J.; Feng, Z.; Gilliland, G.; Bhat, T. N.; Weissig, H.; Shindyalov, I. N.; Bourne, P. E. The Protein Data Bank. *Nucleic Acids Res.* **2000**, *28*, 235-242.

59. *Schrödinger Release 2014-2*: Schrödinger Suite 2014-2 Protein Preparation Wizard; Epik version 2.8, Schrödinger, LLC, New York, NY, 2014; Impact version 6.3, Schrödinger, LLC, New York, NY, 2014; Prime version 3.6, Schrödinger, LLC, New York, NY, 2014.

60. *Small-Molecule Drug Discovery Suite 2014-2*: Glide, version 9.8, Schrödinger, LLC, New York, NY, 2014.

61. Baell, J. B.; Holloway, G. A. New substructure filters for removal of pan assay interference compounds (PAINS) from screening libraries and for their exclusion in bioassays. *J. Med. Chem.* **2010**, *53*, 2719-2740.

62. *Schrödinger Release 2017-2*: Canvas, Schrödinger, LLC, New York, NY, 2017.

63. Stolfa, D. A.; Stefanachi, A.; Gajer, J. M.; Nebbioso, A.; Altucci, L.; Cellamare, S.; Jung, M.; Carotti, A. Design, synthesis, and biological evaluation of 2-aminobenzanilide derivatives as potent and selective HDAC inhibitors. *ChemMedChem* **2012**, *7*, 1256-1266.

64. Marek, M.; Kannan, S.; Hauser, A. T.; Moraes Mourao, M.; Caby, S.; Cura, V.; Stolfa, D. A.; Schmidtkunz, K.; Lancelot, J.; Andrade, L.; Renaud, J. P.; Oliveira, G.; Sippl, W.; Jung, M.; Cavarelli, J.; Pierce, R. J.; Romier, C. Structural basis for the inhibition of histone deacetylase 8 (HDAC8), a key epigenetic player in the blood fluke Schistosoma mansoni. *PLoS Pathog.* **2013**, *9*, e1003645.

65. Fischer, M.; Skowron, M.; Berthold, F. Reliable transcript quantification by real-time reverse transcriptase-polymerase chain reaction in primary neuroblastoma using normalization to averaged expression levels of the control genes HPRT1 and SDHA. *J. Mol. Diagn.* **2005**, *7*, 89-96.